Summer 8-1-2013

GEOMETRY AND EVOLUTION OF FOLD STRUCTURES WITHIN THE HIGH FOLDED ZONE: ZAGROS FOLD-THRUST BELT, KURDISTAN REGION-IRAQ

Mjahid Zebari
University of Nebraska-Lincoln, mmhzeb@huskers.unl.edu

GEOMETRY AND EVOLUTION OF FOLD STRUCTURES WITHIN THE HIGH FOLDED ZONE: ZAGROS FOLD-THRUST BELT, KURDISTAN REGION-IRAQ

by

Mjahid Zebari

A THESIS

Presented to the Faculty of

The Graduate College at the University of Nebraska

In Partial Fulfillment of Requirements

For the Degree of Master of Science

Major: Earth and Atmospheric Sciences

Under the Supervision of Professor Caroline M. Burberry

Lincoln, Nebraska

July, 2013

GEOMETRY AND EVOLUTION OF FOLD STRUCTURES WITHIN THE HIGH FOLDED ZONE: ZAGROS FOLD-THRUST BELT, KURDISTAN REGION-IRAQ

Mjahid Zebari M.S.

University of Nebraska, 2013

Advisor: Caroline M. Burberry

Understanding the deformation style within the Zagros Fold-Thrust Belt is crucial for understanding the convergence between the colliding Arabian and Eurasian plates and nature of structures that trap hydrocarbons within the belt. The Zagros Fold-Thrust Belt has propagated ~250 km southwest-ward in Northern Iraq. In this study, deformation style of a number of fault-related folds within a part of the belt has been considered. The research intends to understand the geometry and formation mechanisms of these folds, via constructing models for the deformation geometry of folds and associated thrusts at depth using field data and seismic lines and detecting their growth using geomorphic criteria. Aspect ratio of the folds and fold symmetry index were used to categorize fault-related folds. The estimated depth of the detachment level within the sedimentary cover was considered.

Folds in the area are broad and box-shaped with close to gentle inter-limb angles and spaced at wavelengths of 5-10 km. The aspect ratio and the fold symmetry index imply that the folds are transitional between fault-bend folds and fault propagation folds. Thick carbonate units in addition to the geometry of related faults govern the broadness and wavelength of the folds. The main detachment level was estimated to be within the Triassic units and the geomorphology of the folds suggests some basement involvement

via reactivated basement faults. Thus, cross-sections are constructed with the main structures as fault-bend or fault-propagation folds down to the Triassic level. Geomorphological criteria along folds point to variations along strike and northwest-ward growth of the northwestern side of the Harir, Shakrok/Khatibian, Safin and Bani Bawi/Pirmam Anticlines. Lateral growth of folds is constrained by presence NE-SW oriented strike-slip basement faults. Clear understanding of fold/thrust geometries leads to improved predictions of trapping potential in individual structures in the area. Traps may be segmented via lateral growth of folds and/or influence of basement faults. Comprehending the deformation of sedimentary cover (especially thrust geometry and detachment levels) requires further investigations.

Acknowledgments

I gratefully appreciate the scholarship from the Human Capacity Development Program (HCDP) of Kurdistan Region Government. I would like to thank the University of Nebraska-Lincoln, Department of Earth and Atmospheric Sciences for providing the essential facilities to conduct the research. I am thankful to the Salahaddin University, Geology Department and Dr. Ahmed Aqrawi (the department chair) for their support and assistance during the field work. I appreciate the academic license of Move Software from Midland Valley.

I would like to express my sincerest gratitude to my advisor Dr. Caroline Burberry for her immense guidance and advices and encouragement throughout the period of the study. I would like also to extend my gratitude to Dr. Tracy Frank and Dr. David Watkins for being a part of the committee. I have special thanks to Mr. Irfan Asaad for his efforts and being a link between me and the HCDP.

I express my great gratitude to my friends Mala, Hadi, Jalal, Mikaiel, Naman, Emad, Sanan, Edris, Ayas, Edris, and Hushiar for their help during the field work. I would like to thank Bobbi Brace for linguistic reviewing. Finally, my greatest gratitude goes to my parents and family for their personal support and patience.

IN THE LOVELY MEMORY OF MY SISTER

NAJLA

CONTENTS

1-INTRODUCTION

1.1 Importance of the Zagros Fold-Thrust Belt

Fold-thrust belts mark the deformation fronts of the major orogens that form from colliding plates (Twiss and Moores, 2007). The shortening observed in the fold-thrust belts is due to the convergence between colliding plates (Marshak and Wilkerson, 2004). The fold-thrust belts can disclose information about the amount of shortening, direction of convergence, timing of deformation and additional factors involved in the deformation via understanding its deformation style, i.e. deformation intensity, fold spacing, displacement along faults and major structural trend.

The Zagros Fold-Thrust Belt extends approximately 2000 km from SW Iran to the Kurdistan Region (N Iraq) and SE Turkey. It formed as a result of the Zagros Orogeny due to collision between the Arabian and Eurasian plates, which started in the Late Cretaceous. The folding due to convergence in the Zagros Fold-Thrust Belt may have started in the Eocene and have propagated southwestward in the Pliocene (Hessami et al., 2001; Csontos et al., 2012). The Zagros Fold-Thrust Belt is a key region for understanding convergence between the Arabian and Eurasian tectonic plates. The deformation style of the Zagros Fold-Thrust Belt has been intensively studied southeastern segments in Iran while there are few comprehensive studies about the northwestern segment in the Kurdistan Region, which is the main motivation for this study.

It is estimated that fold-thrust belts hold 14% of the discovered and 15% of the undiscovered global recoverable hydrocarbons. Furthermore, the Zagros Fold-Thrust Belt

holds 49 % of global fold-thrust belt hydrocarbons (Cooper, 2007). Structures within the Zagros Fold-Thrust Belt comprise immense hydrocarbon traps. Recently, the NW segment of the belt in the Kurdistan became a region of interest for hydrocarbon exploration. Hydrocarbons are trapped within anticlines and related structures. Consequently, understanding the deformation style and development of these folds and associated faults in this area is crucial in the exploration.

This study addresses the geometry and evolution of a number of fold structures within the High Folded Zone, which is a part of the northwestern segment of the Zagros Fold-Thrust Belt in the Kurdistan Region, through constructing of structural cross-sections and detecting fold growth. The study is carried out using field data and remote sensing tools, as well as the construction of mechanically viable balanced cross-sections.

1.2 Aim of the study

The overall aim of the present study is to address the geometry and formation mechanisms of a number of fault-related folds within a part of the Zagros Fold-Thrust Belt known in Northern Iraq as the High Folded Zone. This will be done by constructing models for the deformation geometry of specific folds and their associated thrusts at depth. The study also aims to identify possible detachment levels at depth and to estimate shortening across the folds in the area. The last aim is to understand along strike variations in fold segments and their lateral growth via variations in geomorphic criteria along the folds.

The motivation of this study is that the hydrocarbon traps in the area are closely related to fold structures. Consequently, understanding geometry and categories of folds,

fold segments, geometry of related-thrusts and cutoffs of the geological units will provide better predictability and understanding of structural traps within the folds.

1.3 Geographic Location of the Study Area

The study area covers about 4000 km^2 within in the Kurdistan Region, Northern Iraq (Figure 1-1). The area is located within the Erbil and Dohuk governments. The Kurdistan Region is located in the northeastern corner of the Arabian Plate. Structurally the area is located within the northwestern segment of the Zagros Fold-Thrust Belt. The studied folds include Pirmam, Bani Bawi, Safin, Shakrok, Khatibian and Harir Anticlines in the east and Aqra, Perat and Peris Anticlines in the west. The regional geology of the study area is discussed in detail in chapter 2.

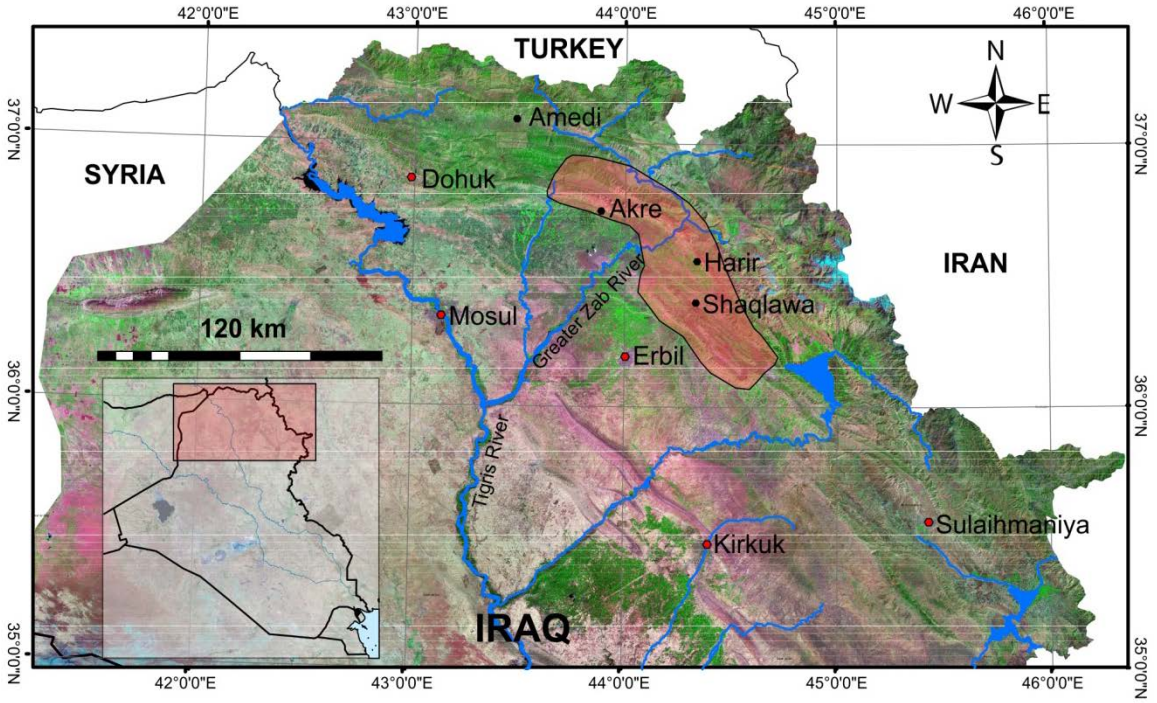

Figure 1-1: Map of Northern Iraq denoting geographical location of the study area (red polygon).

2-REGIONAL GEOLOGY

2.1 Introduction

As a part of northern Iraq, the study area is located in the northeastern margin of the Arabian Plate. The area underwent the tectonic events that affected northeastern part of the Arabian plate. Northern Iraq is divided to a number of zones based on the structural elements of each (specifically intensity and style of deformation), which are mostly related to the Zagros convergence (Jassim and Goff, 2006; Aqrawi et al., 2010). In this chapter, an overview of the tectonic development of the northeastern part of the Arabian Plate and the structural trend and stratigraphy of the High Folded Zone including the study area will be discussed.

2.2 Tectonic Development of N Iraq

The Arabian Plate was affected by the Nabitah Orogeny from 680 to 640 Ma (Stern and Johnson, 2010). N-S trending faults that formed from E-W compression of the Nabitah Orogeny are conspicuous in the basement of S and W Iraq and less common in N Iraq (Jassim and Goff, 2006). Subsequently, in the Late Precambrian, the NW-SE trending Najd rifting event (610-520 MA) started. This formed the NW-SE trending Najd fault system in Iraq, which is prominent in the basement of N Iraq and it influences the boundaries of tectonic zones in northern Iraq (Jassim and Goff, 2006).

Throughout most of the Paleozoic, the area formed a series of intracratonic basins receiving siliciclastic sediments. N-S trending grabens and tilted fault blocks were formed in the Arabian Platform during the Cambrian-Carboniferous due to the back-arc extensional phases of the Caledonian (~435-365 Ma) and Hercynian (~364-295 Ma)

Orogenies (Sharland et al., 2001; Ibrahim, 2009). The area was located within a back-arc setting during the Hercynian Orogeny in the Carboniferous. In the Permian the Arabian Plate underwent crustal extension (rifting) which led to separation of the Iranian Terranes, and spreading of the Neo-Tethys Ocean. The area became a post-rift passive margin to the SW of the Neo-Tethys Ocean from the late Permian to Cretaceous (Sharland et al., 2001).

Subduction between the Arabian and the Eurasian plates led to the Zagros Orogeny. The orogeny started in the Late Cretaceous by ophiolite obduction on the margin of the Arabian Plate (Yilmaz, 1993; Blanc et al., 2003; Ghasemi and Talbot, 2005). The continental collision started in the Miocene in the southeastern part of the orogen and in the Oligocene in its northwestern part. The collision led to closure of the Neo-Tethys Ocean (Blanc et al, 2003). The velocity of the Arabian Plate movement toward the Eurasian Plate, considered as a fixed plate, is estimated at 16-22 mm/yr (Figure 2-1; Sella et al, 2004).

2.3 Zagros Fold-Thrust Belt

The Zagros Fold-Thrust Belt is a result of subduction between the Arabian and the Eurasian plates. The belt extends about 2000 km from the Hormuz Strait, southwestern Iran to the Kurdistan Region-Iraq and SE Turkey (Figure 2-1) and covers the northeastern deformed part of the Arabian plate (Alavi, 2004 and 2007). The deformation has propagated 250-350 km southwestward in the northeastern margin of the Arabian Plate toward the Mesopotamian foreland basin and the Arabian Gulf (Figure 2-1). NE-SW directed convergence occurs across the belt, except in its northwestern part, which exhibits N-S directed convergence. This is achieved by a combination of NE-SE

convergence and right-lateral strike-slip fault along the Zagros Suture (Talebian and Jackson, 2002; Allen el al, 2004). Shortening across different sectors of the Zagros Fold-Thrust Belt is estimated at 16-30 % in Iran (Alavi, 2007), and at 33 % in the Kurdistan Region (Ibrahim, 2009).

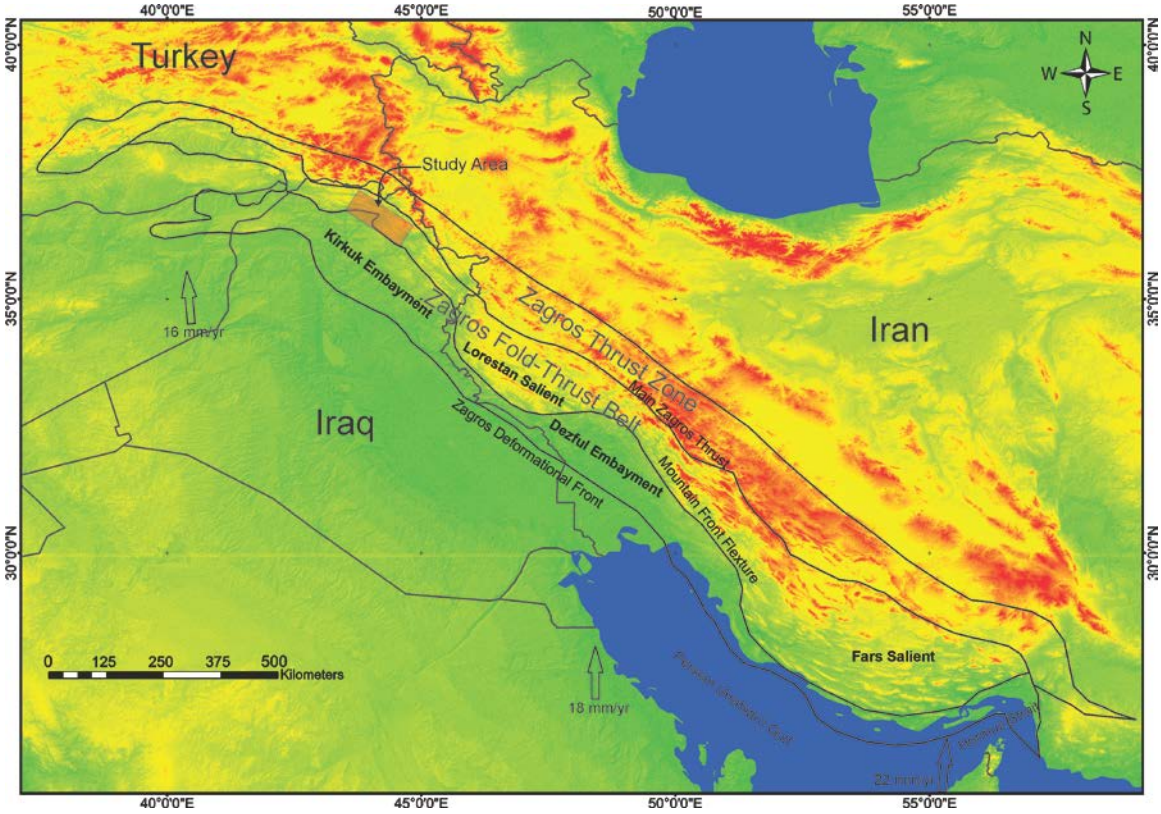

Figure 2-1: Physiographic map of the Zagros showing main subdivisions and longitudinal segments of the belt, and relative velocities of the Arabian Plate movement toward a fixed Eurasian plate (Sella et al., 2002).

Longitudinally, the Zagros Fold-Thrust Belt is divided into number of segments. These segments include the Fars Salient, Dezful Embayment and Lorestan Salient in Iran, and the Kirkuk Embayment in Iraq (Figure 2-1). The deformed wedge includes both cover strata and basement rocks (Alavi, 2007). Large-scale variations in the geometry of the deformed wedge in the different segments of the belt are controlled by both

mechanical stratigraphy of the sedimentary cover and basement involvement (McQuarrie, 2004; Alavi 2007). The presence of salt beneath the Fars and Lorestan regions led the deformation to propagate more foreland-ward. On the other hand, there is no evidence of salt beneath the Dezful and Kirkuk embayments and thus deformation of the belt propagated a shorter distance (McQuarrie, 2004).

2.4 Tectonic Subdivisions of Iraq

Iraq is located in the northeastern part of the Arabian Plate. Deformation due to the Zagros Orogeny has propagated southwestward through north and northeastern parts of Iraq. Many authors (e.g. Buday and Jassim, 1987; Numan, 1997; Jassim and Goff, 2006) have subdivided Iraq into a number of tectonic zones. These subdivisions are based on tectonic and structural elements. Most of them subdivide Iraq into the stable shelf (unfolded zone that covers of central and southern Iraq), the unstable shelf (folded and thrusted zone that covers northern and northeastern parts of Iraq, includes the study area) and the Zagros Suture. The tectonic subdivision of Jassim and Goff (2006) is the most recent one. Based on their tectonic subdivision the study area is located within a part of the High Folded Zone (Figure 2-2).

2.4.1 Foothill (Low Folded) Zone

The Foothill Zone covers the Kirkuk Embayment and other northwestern parts of Iraq. Its southern boundary with the Stable Shelf runs along southern limb of the first major surface anticline (Zagros Deformational Front). Its northern boundary with the High Folded Zone runs along the southern limb of the first high anticlines (Jassim and Goff, 2006). The Foothill Zone is dominated by low amplitude folds with high wavelengths and it shows low relief topography. Eocene rocks are the oldest exposed

Formations in the area (Csontos et al., 2012). It is divided into a number of subzones (Figure 2-2).

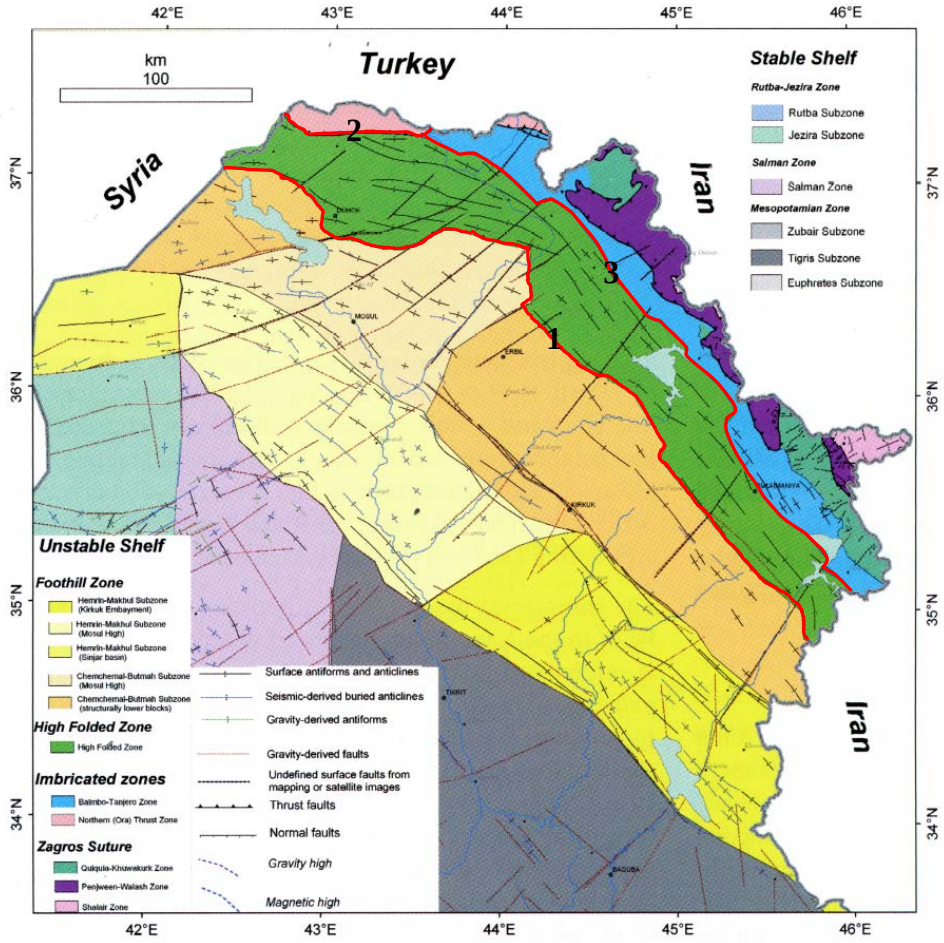

Figure 2-2: Tectonic subdivision of northern Iraq with the main structural trend (Jassim and Goff, 2006). Red lines are thrusts that bound the High Folded Zone; 1) Mountain Front Flexure, 2) Ora Thrust and 3) High Zagros Reverse Fault. Mountain Front Flexure and High Zagros Reverse Fault are extended to the Iranian Zagros.

2.4.2 High Folded Zone

The study area is located within the High Folded Zone. The south and southwest boundary of the zone runs along the south and southwest limb of the first high anticlines and coincides with a deep seated thrust fault (Mountain Front Flexure). This separates the

High Folded Zone from the Foothill Zone. The north boundary is the Ora (Northern) Thrust, while the northeast boundary is more complex and runs along a thrust fault and (High Zagros Reverse Fault) separates it from the Balambo-Tanjero Zone (Figure 2-2). The thrust faults that make the zone's boundary are interpreted to be the surface expressions of buried reactivated basement faults from the NW-SE trending Najd Fault System (Ameen, 1992; Jassim and Goff, 2006; De Vera et al., 2009).

The width of the High Folded Zone ranges from 25 to 50 km. The folds in this zone are oriented on a NW-SE trend in northeastern Iraq and E-W trend in northern Iraq. The folds are mostly asymmetrical with steeper S- or SW-dipping limbs and sometimes with thrust fault in the steeper limb (Jassim and Goff, 2006). Topographic relief and intensity of deformation increase northeastward from the foreland to the Main Zagros Thrust.

The depth of the Precambrian basement in the High Folded Zone, which is derived from gravity data and thickness of the sedimentary megasequences ranges from 6 to 9 km (8 km on average). Cretaceous rocks (mostly carbonates) are exposed in the cores of some anticlines; while Tertiary rocks (clastic and carbonates) fill the adjacent synclines. The High Folded Zone was uplifted during the Oligocene and as a result, Oligocene formations are absent in the area (Jassim and Goff, 2006).

2.4.3 Imbricated Zone

The Imbricated Zone is a narrow belt (15 km in the north 25 km in the northeast) that covers areas north and northeast of the High Folded Zone (Figure 2-2). It is intensively folded and thrusted. Anticlines are dislocated by thrusts into imbricates and override synclines. It is separated from the Zagros Thrust Zone, where ophiolite nappes

and related deep-sea sediments are emplaced (Csontos et al., 2012), by the Main Zagros Thrust. The Imbricated Zone is subdivided into: i) Balambo-Tanjero Zone in the northeast, and ii) Ora (Northern) Thrust Zone in the north.

2.5 Precambrian Basement

The Precambrian basement is neither exposed nor penetrated by wells in Iraq. In addition, there is a lack of detailed geophysical data (such as aeromagnetic and bouguer gravity) in the High Folded Zone. Thus, the depth and composition of the Precambrian basement in the High Folded Zone are poorly understood. The depth of the basement has been inferred from the thickness of sedimentary sequences and sparse regional gravity data (Jassim and Goff, 2006). In general, the depth of basement is estimated to be ac. 8 km in depth on average (Jassim and Goff 2006). Ameen (1992) used satellite image interpretation to subdivide the basement in Northern Iraq into two blocks with a number of sub-blocks (figure 2-3). The Mosul Block, with WNW-ESE trending longitudinal faults, is located to the northwest of the Greater Zab River. The Kirkuk Block, with NE-SW trending longitudinal faults, is located to the SW of the Greater River. A regional basement fault (right lateral, strike slip; in the Transversal Fault System) that runs along the river separates these two blocks. Due to series of uplifts and erosional/non-depositional gaps during the Jurassic and Cretaceous in the Mosul Block, its sedimentary cover is thinner than the Kirkuk Block's sedimentary cover (Ameen, 1992). The composition of the basement in the High Folded Zone is still undefined. The basement rocks in parts of the Foothill Zone that are adjacent to the High Folded Zone are composed of the post-tectonic gabbro, diorite and granite (Jassim and Goff 2006).

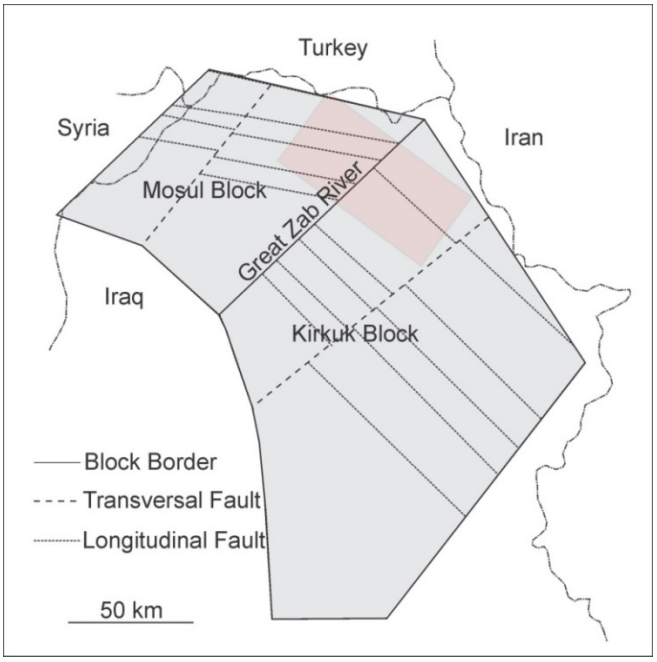

Figure 2-3: basement fault blocks in the northern Iraq (Ameen, 1992).

2.6 Structural Geology of the High Folded Zone

The High Folded Zone is a lateral extension of the Zagros Simple Fold Belt in Iraq. The dominant feature of the zone is the orogenic curvature with ~30° bend (Csontos et al., 2012). The folds trend in a northeast-southwest direction in the eastern segment and nearly east-west direction in the western segment (Figure 2-2). The fold trend changes abruptly along the Greater Zab River. The river terrace is interpreted as a lineament representing a right-lateral basement fault (Ameen, 1992; Omar, 2005; Jassim and Goff, 2006). In addition to the curvature, high folds propagate further toward the foreland on the eastern side than on the western side.

The zone is dominated by en-echelon, long, linear, doubly plunging fault-related folds. The folds are dominantly southwest verging and have been deformed on multiple detachments (De Vera et al., 2009). The hinge length of the folds varies from 25 to 70 km, and fold wavelengths vary from 5 to 10 km. Most folds are box-shaped with a broad

hinge area. This is probably caused by folding of thick Cretaceous carbonate layers. The folding creates a space problem in both outer and inner arcs of the fold. The outer layers accommodate layer parallel elongation, which may be associated with normal faults and crestal collapse; whereas, inner layers may accommodate shortening and internal thrusting (Csontos et al., 2012). The High Folded Zone folds are usually associated with thrust faults in their southern limb. Surface extension of the faults is limited to the northeastern part of the zone. Displacement along these thrusts may reach 3 km such as the thrust that makes the southern boundary of the zone, which is an extension of the basement fault from the Najd Fault System (Jassim and Goff, 2006). This boundary is termed Mountain Front Flexure in the Zagros Fold-Thrust Belt (Berberian, 1995).

2.7 Lithostratigraphy of the High Folded Zone

In the High Folded Zone, the sedimentary cover generally consists of rock units of Paleozoic (1.5-5 km thick), Triassic (1.5-2 km thick), Jurassic (1.1 km thick), Cretaceous (1.05-2 km thick), Palaeogene (1-1.5 km), and Neogene sediments which fill some synclines in the area with a variable thickness (Figure 2-4; Jassim and Goff, 2006). The exposed rocks in the core of the anticlines are mostly Cretaceous, while Jurassic and Triassic rock units crop out in anticlines that are close to the Imbricated Zone. Cenozoic rock units form the core of the synclines. These synclines are sometimes covered by Quaternary sediments. Based on the mechanical properties, the sedimentary cover units in the Zagros Fold-Thrust Belt in Iran (Colman-Sadd, 1978; Sherkati et al., 2005) and in the Kirkuk Embayment in Iraq (Kent, 2010).have been divided into the lower mobile group, the competent group, the upper mobile group, and the incompetent group from the base to the top, analogous to the typical divisions made in Iran,

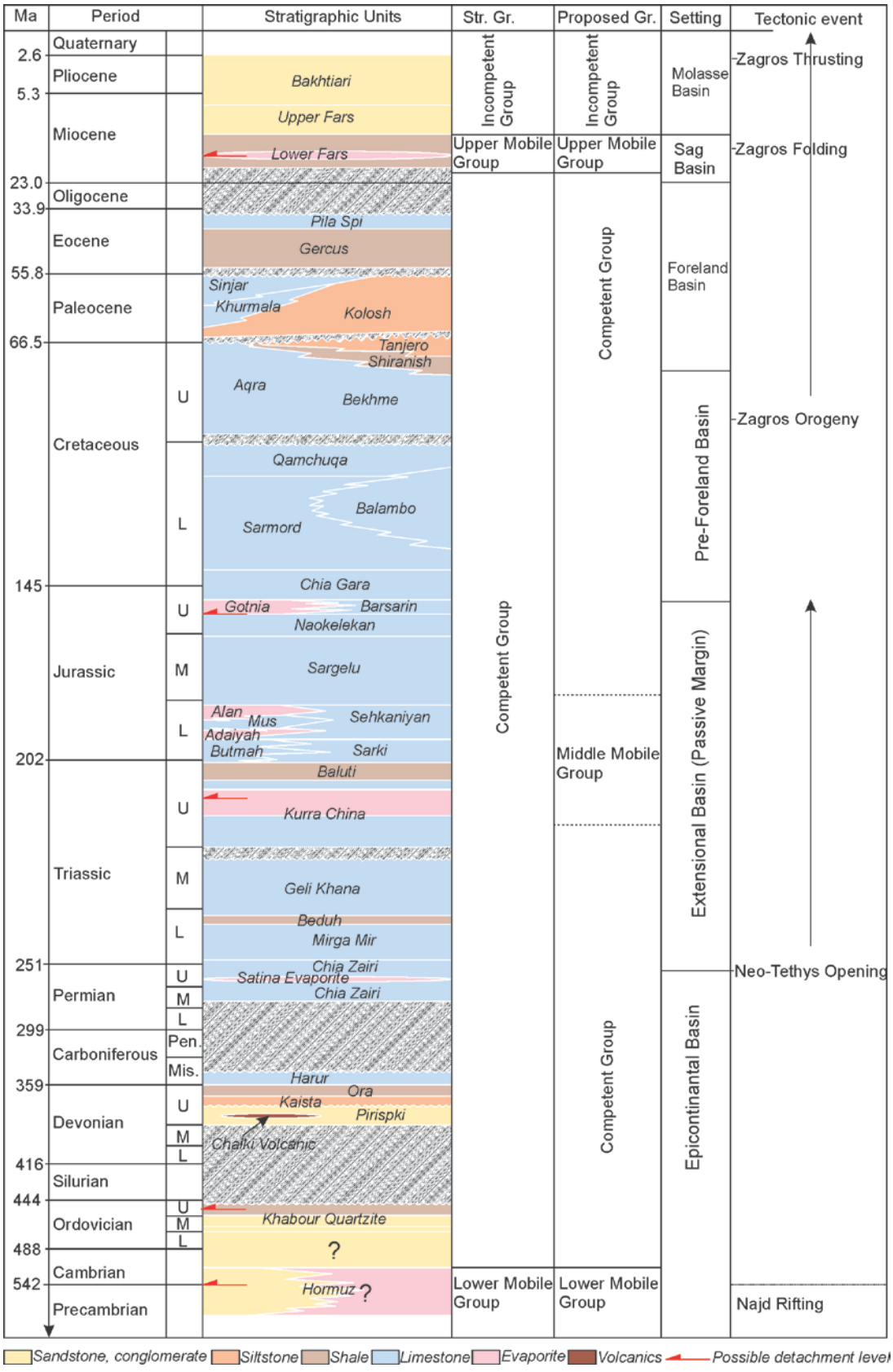
Ma
Period
Stratigraphic Units
Str. Gr.
Proposed Gr.
Setting
Tectonic event
Quaternary
Pliocene
Miocene
Oligocene
Eocene
Paleocene
Cretaceous
Jurassic
Triassic
Permian
Carboniferous
Devonian
Silurian
Ordovician
Cambrian
Precambrian
2.6
5.3
23.0
33.9
55.8
66.5
145
202
251
299
359
416
444
488
542
U
M
L
Pen.
Mis.
Bakhtiari
Upper Fars
Lower Fars
Pila Spi
Gercus
Sinjar
Khurmala
Kolosh
Tanjero
Shiranish
Aqra
Bekhme
Qamchuqa
Balambo
Sarmord
Chia Gara
Gotnia
Barsarin
Naokelekan
Sargelu
Alan
Mus
Adaiyah
Butmah
Sehkaniyan
Sarki
Baluti
Kurra China
Geli Khana
Beduh
Mirga Mir
Chia Zairi
Satina Evaporite
Harur
Ora
Kaista
Pirispki
Chalki Volcanic
Khabour Quartzite
?
Hormuz ?
Incompetent Group
Upper Mobile Group
Competent Group
Lower Mobile Group
Incompetent Group
Upper Mobile Group
Competent Group
Middle Mobile Group
Competent Group
Lower Mobile Group
Molasse Basin
Sag Basin
Foreland Basin
Pre-Foreland Basin
Extensional Basin (Passive Margin)
Epicontinantal Basin
Zagros Thrusting
Zagros Folding
Zagros Orogeny
Neo-Tethys Opening
Najd Rifting
Sandstone, conglomerate
Siltstone
Shale
Limestone
Evaporite
Volcanics
Possible detachment level

Figure 2-4 (page 13): The stratigraphic column of the study area (Paleozoic units; modified after Al-Juboury and Al-Hadidy, 2009; Mesozoic and Cenozoic units modified after Jassim and Goff, 2006; Csontos et al., 2012) showing stratigraphic groups based on their mechanical properties (Kent, 2010) with a proposed subdivision of stratigraphic units for the area, basin setting (Ibrahim, 2009), and major tectonic events (Sharland et al., 2001, Csontos et al., 2012; Sissakian, 2013).

2.7.1 Lower Mobile Group

The lower mobile group includes the Infra-Cambrian Hormuz Salt, which was deposited in a series of north-south trending grabens in the eastern Arabian Plate. The Hormuz is dominantly composed of halite facies. The halite facies change to marine dolomite facies northward and to sandstone and shales northwestward in southeastern Turkey (Figure 2-5). Infra-Cambrian units, which were deposited in the west and northwest extensions of the Hormuz Basin in southeastern Turkey, are clastics. Thus, the presence of the Hormuz Salt has not been observed in the Kirkuk Embayment (Kent, 2010). McQuarrie (2004), Bahroudi and Koyi (2003) and others propose that large-scale variation in the geometry of the Zagros Fold-Thrust Belt is controlled by presence of the Hormuz Salt, which acts as a decollement and occurs beneath the Lorestan and Fars regions, but is not thought to occur beneath the Dezful and Kirkuk embayments.

2.7.2 Competent Group

The competent group includes sedimentary units that range from the Cambrian to the Oligocene. Middle Ordovician-Lower Carboniferous units, which are present as outcrops in the Ora Thrust Zone (NW of the study area), consist of clastic sedimentary rocks (sandstone, siltstone, and shale) with rare carbonate, and were deposited in intracratonic basins (Numan, 1997). In addition to studied units in the Ora Zone, Jassim and Goff

(2006) and Kent (2010) predicted the presence of other buried units below the cropped out units in the Ora Thrust Zone, by correlation with studied formations of the same age in neighboring countries (NE Syria and SE Turkey). Lower Carboniferous-Upper Cretaceous units consist of carbonates with shales with evaporites. Most of these carbonate units were deposited in carbonate platforms in the northeastern passive margin of the Arabian Plate. Upper Cretaceous-Miocene units consist of clastic rocks interbedded with some units of carbonate (Bellen et al. 1959; Jassim and Goff, 2006; Aqrawi et al., 2010). Within the competent group, Triassic-Jurassic anhydrites and Ordovician-Silurian shales may act as possible detachments in the area.

2.7.3 Upper Mobile Group

The upper mobile group includes the *Lower Fars Formation* (Middle Miocene) (Kent, 2010). Its thickness varies from 300 m to 900 m in Kurdistan. It is composed of basal conglomerate overlain by transitional beds of anhydrite, mudstone, siltstone and sandstone with limestone beds (Bullen et al., 1959, Jassim and Goff, 2006). The Lower Fars Anhydrite acts as a detachment surface in the Foothill Zone.

2.7.4 Incompetent Group

The incompetent group in Iraq includes the *Upper Fars Formation* and *Bakhtiari Group* (Kent, 2010). The *Upper Fars Formation* (Late Miocene) consists of alternating beds of red mudstone, marls, siltstone and sandstone. The *Bakhtiari Group* (Late Miocene-Late Pliocene) is composed of fining upwards cycles of gravelly sandstone, cross-bedded sandstone, coarse and thick fluviatile and estuarine conglomerates. Quaternary sediments, which consist of residual and terrace gravels, overlie the *Bakhtiari Group* (Bullen et al., 1959, Jassim and Goff, 2006).

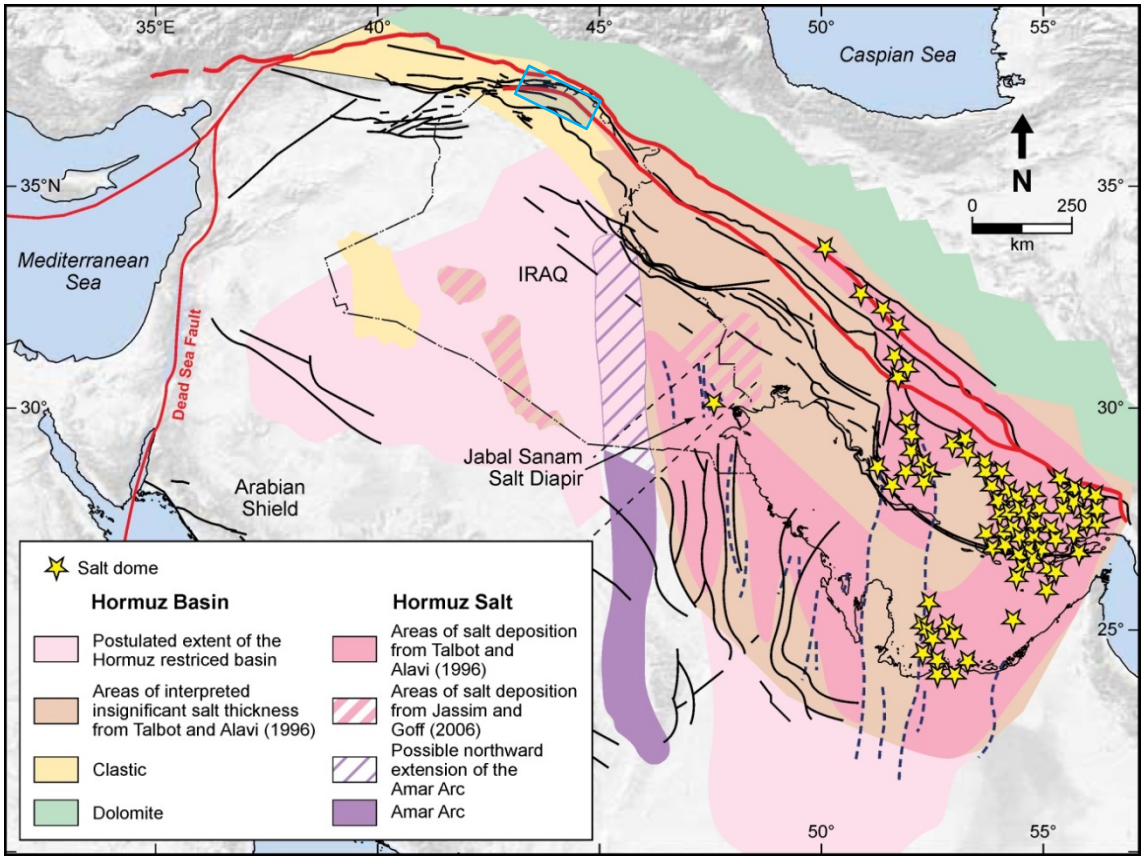

Figure 2-5: Infra-Cambrian Hormuz Salt Basins showing distribution of Hormuz facies, which change from salt facies to dolomite facies northward and to clastic facies northwestward to northern Iraq and southeastern Turkey; the blue square denotes the location of the study area (Kent, 2010).

3-METHODS

3.1 Introduction

The study was done using structural cross-sections constructed from data acquired in the field. The thickness and lithology of subsurface strata were measured directly from field or obtained from the literature. Geometry of folds and geomorphic features were obtained from satellite images and Digital Elevation Models and used to understand the evolution and lateral growth of folds. Geomorphic indices may help in categorizing fault-related folds and evaluation of involvement of underlying forces (e.g. basement faults) in the deformation.

3.2 Field Work

The field work consisted of mapping and acquiring spatial orientation data along two sections across the macroscale folds. The data include attitude of strata (dip amount and dip direction), geographic locations (latitude, longitude and elevation) using a GPS receiver and lithological boundaries between geological units where it was possible. The sections were selected along the best representative accessible trace across the folds (parallel to the direction of inferred shortening). One is located in the eastern part of the study area in the Shaqlawa District across the Harir, Khatibian, Safin and Pirmam Anticlines in a nearly NE-SW trend. The other is located in the western part of the study area, in the Aqra District across the Perat and Peris Anticlines a in nearly N-S trend. Other geological elements such as mesoscale folds, macro and mesoscale faults, sedimentary unit lithologies and boundaries, and geomorphological features were also observed along each transect.

3.3 Remote Sensing

Remote sensing data, which include Landsat satellite images and Digital Elevation Models (DEMs), were used to calculate geomorphic indices of folds that may help categorizing them and detect geomorphic criteria that indicate fold growth. Remote sensing work was conducted using ArcGIS 10.1 software.

3.3.1 Geomorphic Indices of folds

Landsat satellite images were used in geological mapping and to delineate the outline of folds and fold hinge lines. The Landsat scenes were obtained from the NASA website (https://zulu.ssc.nasa.gov/mrsid). The scene is a Landsat Thematic Mapper image with pixel size of 28.5 m. The color composite of the scene consists of Band 7 (mid-infrared light) as red, Band 4 (near-infrared light) as green and Band 2 (visible green light) as blue and is processed under MrSID compression techniques (Tucker et al., 2004). Folds were delimited based on lithology. Bare clastic rocks appear in pink color in the satellite image while carbonate rocks are lighter and these textures helps to delimit the folds. The Cretaceous carbonates or Eocene Pila Spi Limestone form the core of anticlines and the Cenozoic clastics comprise the adjacent synclines. When the core of an anticline is made up of the Cretaceous carbonates, the Pila Spi Limestone forms a ridge around the anticline (Figure 3-1).

The resultant fold map was used to calculate the geomorphic indices of the folds. Both aspect ratio and fold symmetry index were calculated (Figure 3-2). Aspect ratio is the ratio of the fold hinge length to the width of fold or half wavelength (Cosgrove and Ameen, 2000). Fold symmetry index is equal to the width of forelimb (shorter limb) divided by half-width of the fold (Burberry et al., 2010). These indices can be used to

distinguishing fold types. Detachment folds show low aspect ratios with high symmetry; fault-propagation folds have low aspect ratios with low symmetry, while fault-bend folds show relatively high aspect ratios with low symmetry (Blanc et al., 2003; Burberry et al., 2010). Forced folds are expected to have an aspect ratio of more than 10 (Sattarzadeh et al., 2000; Blanc et al., 2003).

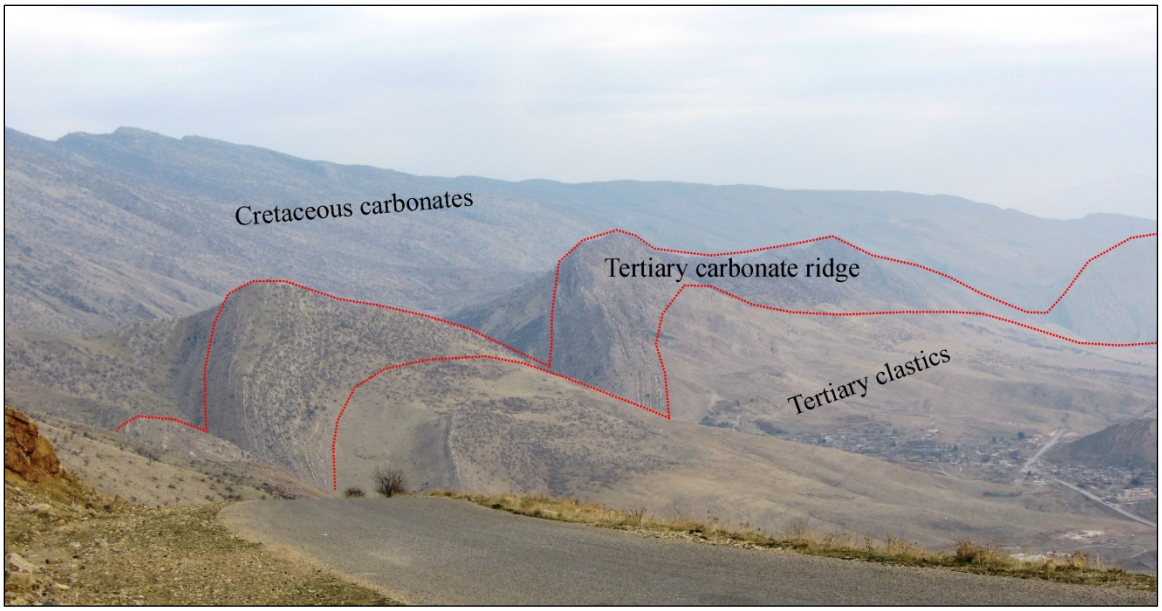

Figure 3-1: Example of stratigraphic distribution across folds in the area (southern limb of the Perat Anticline). The Cretaceous carbonates make up the core of the anticline, Tertiary carbonates make a ridge around the anticlines and the Tertiary clastic rocks fill the adjacent synclines

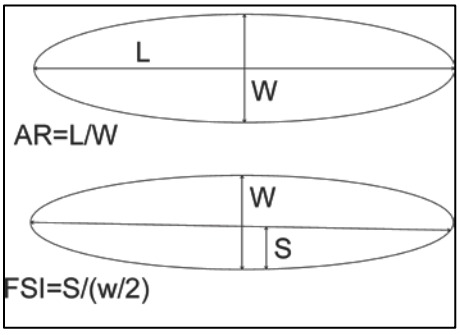

Figure 3-2: Geomorphological indices of the fold, AR=L (length of hinge line)/W (width of the fold), and FSI=S (width of forelimb)/$\frac{W}{2}$ (half width of the fold, that used differentiate fold types (Burberry et al., 2010).

Detachment folds may develop above a detachment or thrust sub-parallel to the bedding. They form from buckling of upper competent strata above ductile strata (Mitra,

2003; Marshak and Wilkerson, 2004). Fault-propagation folds develop from folding of the layers above the tip of the thrust ramp. When slip on the thrust decreases up-section and dies out, the shortening due to thrusting transfers into folding (Mitra, 1990). Fault-bend folds develop from bending of the hanging wall rocks when they move over changes in dip along stepped fault surface (Suppe, 1983; Davis et al., 2011). The preceding categories are very simplified categories of fault-related folds. An evolutionary continuum exists between these categories (Figure 3-3; Cosgrove and Ameen, 2000; Marshak and Wilkerson, 2004; Burberry, 2010). Forced folds are folds in which the overall geometry of the fold is dominated by the shape of some underlying forcing member such as a basement fault (Cosgrove and Ameen, 2000).

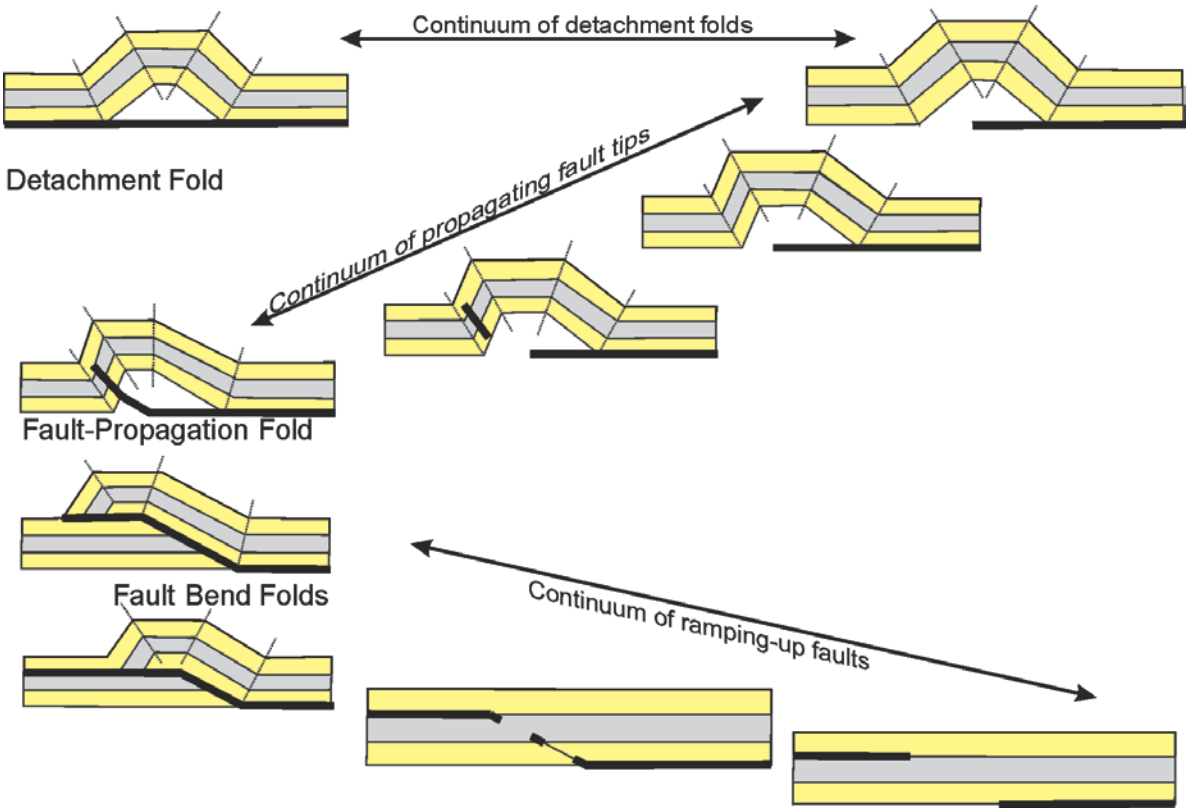

Figure 3-3: Continua of possible fold geometries between the three categories of fault-related fold in cross-section (Burberry et al., 2010).

3.3.2 Geomorphic Criteria that Indicate Fold Growth

Digital Elevation Models (DEMs) were used to constrain and identify additional geomorphic criteria. The DEMs are from the Shuttle Radar Topography Mission (SRTM) and have a spatial resolution of 3-Arc/sec (90 m). These were obtained from USGS Earth Explorer (http://earthexplorer.usgs.gov). DEMs were used to construct the drainage networks in the area and topographic maps (at 100 m contour interval). Topographic profiles along the fold crests and across some specific folds were constructed from the DEMs. Growth of folds was detected by analyzing drainage network on their crests, identifying the location of wind and water gaps, analyzing long topographic profile along fold crests and calculating fold front sinuosity.

In active fold belts, drainage density and dissection decrease toward the newly uplifted parts (Keller et al., 1999) and distinctive asymmetric forked tributary patterns develop. The new patterns develop from pre-existing tributaries, which run parallel to the fold axis in the hinge area toward the direction of fold propagation. Tributaries run toward the growth direction instead of following the steepest topographic gradient perpendicular to the contour lines (Ramsey et al., 2008; Bretis et al., 2011). As folds grow by migration of their hinge and rotation of their limbs, the hinge regions uplift. Drainage basins above the hinge regions are triangular in shape. The tributaries below the hinge regions run, as in principal, down slope perpendicular to the fold axis (Ahmadi et al., 2006; Bretis et al., 2011).

The locations of wind and water gaps were defined through integration of the stream network and topographic maps. In the wind gaps, the topographic high from the fold intersects with an abandoned stream; while in the water gap, the topographic high

from fold intersects with running stream. With the uplift of the fold, stream cuts down through the rocks, creating a water gap across the fold. Water gaps form when the uplifting rates are lower than stream down cutting rates. When the uplifting rates become higher than stream down cutting rates, stream divert from its path around the fold tip leaving the abandoned stream path as a wind gap (Burberry et al., 2010).

There is a decrease in relief of the long topographic profile along the crest of the fold toward the direction of propagation (Jackson et al., 1996; Keller et al., 1999). The younger uplifted parts of the fold tend to be in lower relief in comparison with the older uplifted parts with respect to the exposed stratigraphy.

The fold front lines were delineated from the topographic map and used to calculate fold front sinuosity, which is defined as the ratio between the length of the fold front and length of a straight line approximately parallel to the fold front or fold length; usually the length of the fold axis is used (Figure 3-4; Azor et al., 2002). Within a relatively small region, the time of exposure may vary along different segments of a belt or fold. The older (early uplifted) parts of a fold were exposed to the erosion for a longer time than the younger (later uplifted) parts. Thus, the older parts have been eroded more and consequently they show higher fold front sinuosity (Azor et al., 2002; Burberry et al., 2010).

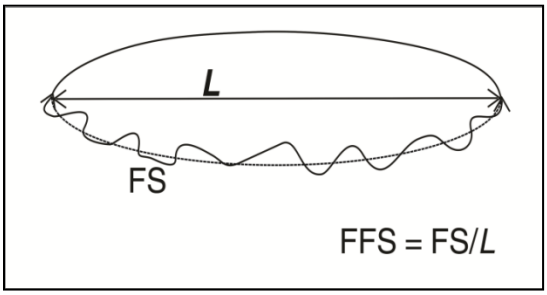

Figure 3-4: Calculation of fold front sinuosity (FFS), which is equal to length of the fold front (FFS) divided by fold length (L). Usually earlier uplifted structures, which have been exposed to weathering processes for longer time, show higher fold front sinuosity (Burberry et al., 2010).

3.4 Constructing Cross-sections

Balanced cross-sections were constructed along the two sections studied in the field, using field data as described above. Kink-band folding style was used in cross-section construction in this study. This style assumes that the cross-section can be divided into a number of dip domains, in which beds have uniform dip. Adjacent domains joint at angular hinges (Marshak and Woodward, 1988). The folds in the eastern side of the area were classified as class 1B with some tendency toward class 1C (Omar, 2005). Class 1B is very close to parallel folding in geometry and the term of parallel folding can be used for class 1A and 1C (Figure 3-5; Ramsey, 1967). Therefore, parallel folding rules were applied in the constructed sections. The horizons were drawn down-section parallel to the dip domains at the surface, while maintaining their constant thicknesses.

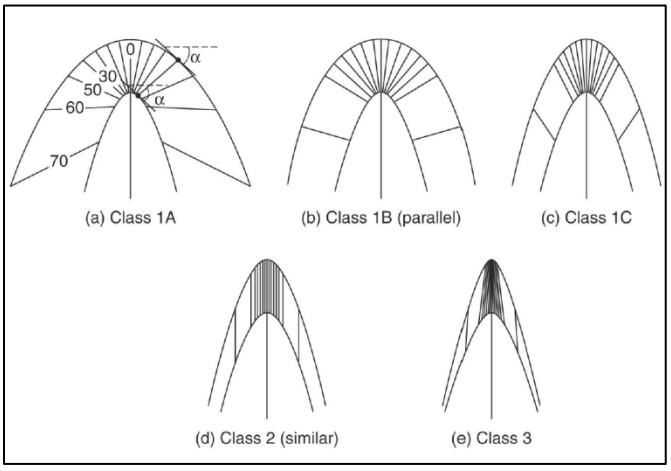

Figure 3-5: Ramsey (1967) classification of fold based on dip isogons. Class 1B is considered as parallel folding and parallel folding term can be used for class 1A and 1C.

Both flexural slip and tangential longitudinal strain folding mechanisms were expected in different structures (Csontos et al., 2012; Frehner et al., 2012; Reif et al, 2012). In flexural slip folding, the shear is not distributed uniformly across the folding layers, but it is concentrated along interfaces or incompetent layers between competent layers, which in the study area are mostly carbonates. Maximum slip occurs on the limbs

and decreases to zero at the hinge (Twiss and Moores, 2007). In tangential longitudinal strain folding, the outer set of layers is stretched while the inner set of layers are shortened and the two sets are separated by a neutral surface (Fossen, 2010).

In depth, faults are drawn based on available seismic lines, geomorphic indices of folds and presence of angular hinge points in the section profile. A number of publically available seismic lines are used to understand the deformation style of nearby fault-related folds and the geometry of associated faults. The same deformation style is used in the constructed cross-sections in the adjacent folds.

Cross-sections were restored using the line length and area balancing methods. Section horizons were restored maintaining their original length and then maintaining the area of units in the sections. The pin lines, which are reference lines placed in a less deformed part of the section to track cross-section restoring (Marshak and Woodward, 1988), are positioned in the southern end of the section because the strata in these locations are only slightly tilted and they most closely resemble the regional dip. Loose lines, which are a reference lines in the trailing end of the section used to track displacement along beds (Marshak and Woodward, 1988), are placed in the trailing edge of section (i.e. their northern end). The cross-sections were constructed and restored using Midland Valley 2D Move 2012.1 software.

After restoring cross-sections, the shortening rates along the sections were measured by using an equation:

$$S = \frac{L° - L}{L°}$$

Where S is the shortening rate, L° is the original (pre-deformed) length of the section, and L is the current (deformed) length of the section (Hossack, 1979).

3.4.1 Detachment Depth

A simplified area balancing method (Figure 3-6) was used to calculate the approximate depth to the detachment beneath different fold structures. In this method, the area of folded rocks raised above a datum is equal to the area of rock which enters to the section due to shortening (Davis et al., 2011). The depth of the detachment is equal to the area of rock entering the section divided by the amount of shortening.

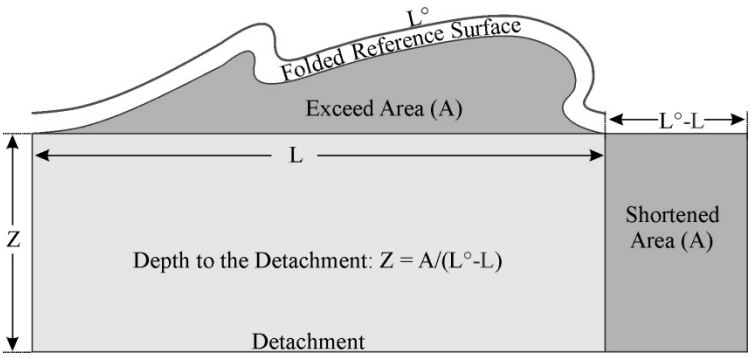

Figure 3-6: Calculating depth to the detachment using area balancing method (Mitra and Namson, 1989)

1.3.3.2 Assumptions

The cross-sections were drawn using a number of assumptions. The simple assumption in constructing balanced cross-sections is that the area of any geological unit is the same before and after deformation, despite tectonic compaction and elongation along strike (Hossack, 1979). However, we know this is untrue, but it is presently not possible to accurately constrain volume loss within the layers; therefore, these are minimum estimates of shortening. Also, the thickness of the stratigraphic units is assumed to be the same before and after deformation. Thickness of sedimentary units is assumed to be constant along individual sections. Finally, the main detachment is

assumed to be located within the Triassic or older units, after the depth to the detachment has been calculated using the area balancing method described above.

1.3.4 Thickness of Stratigraphic Units

In the Shaqlawa Section, the oldest exposed unit is the Upper Cretaceous Bekhme Formation; while in the Akre Section, the oldest exposed unit is the Lower Jurassic Sarki Formation. Thickness of the exposed units was calculated directly from collected field data. The thickness of stratigraphic units which are not exposed along the trend of sections is obtained from the literature (Table 3-1). Due to increasing uncertainties in the thicknesses of stratigraphic units, the presence of detachments and geometry of associated faults, the sections were constructed down to Upper Triassic units.

Table 3-1: Thickness of stratigraphic units used in construction of cross-sections; bold numbers are from field data, regular font numbers are from literature (Jassim and Goff, 2006; Aqrawi et al., 2010).

Stratigraphic Unit	**Shaqlawa Section (m)**	**Akre Section (m)**
Lower Fars	**320**	**350**
Pila Spi	**80**	**80**
Gercus, Kolosh, Khurmala, Shiranish and Tanjero	**1030**	**150**
Aqra, Bekhme and Qamchuqa	800	**800**
Balambo, Garagu and Sarmord	700	**500**
Chia Gara, Barsarin, Naokelekan and Sargelu	550	**350**
Sehkaniyan and Sarki	480	480
Baluti and Kurra China	900	900

4-RESULTS: DEFORMATION STYLE

4.1 Introduction

Structural cross-sections, constructed from integrated field data that have been acquired during the field season, publicly available seismic data, and geomorphic features of folds that have been calculated from satellite images, are used to understand the geometry and formation mechanisms of folds and the associated thrusts in the study area and detect growth of folds. The displacement along thrusts was measured. Then, the cross-sections were restored using both line length balancing method and area balancing method to test the validity of the structures, and to estimate shortening along the sections.

4.2 Results from Field Observations

In the Shaqlawa Section, data were collected across the Pirmam, Safin, Khatibian, and Harir Anticlines. The Bekhme (U. Cretaceous), Shiranish (U. Cretaceous), Kolosh (Paleocene-L. Eocene), Gercus (Middle Eocene), Pila Spi (U. Eocene), Lower Fars (M. Miocene) and Upper Fars (U. Miocene) Formations, as well as a lens of Khurmala within the Kolosh Formation, crop out along the section. In the Akre Section, data were acquired across the Perat and Peris Anticlines. The exposed strata include the Sarki (L. Jurassic), Sehkaniyan (L. Jurassic), Sargelu (M. Jurassic), Naokelekan (U. Jurassic), Barsarin (U. Jurassic), Chia Gara (U. Jurassic-L. Cretaceous), Sarmord (L. Cretaceous), Qamchuqa (L. Cretaceous), Aqra (U. Cretaceous), Kolosh (Paleocene-L. Eocene), Khurmala (Paleocene-L. Eocene), Gercus (M. Eocene), Pila Spi (U. Eocene), Lower Fars (M. Miocene) and Upper Fars (U. Miocene) Formations (Figure 4-1).

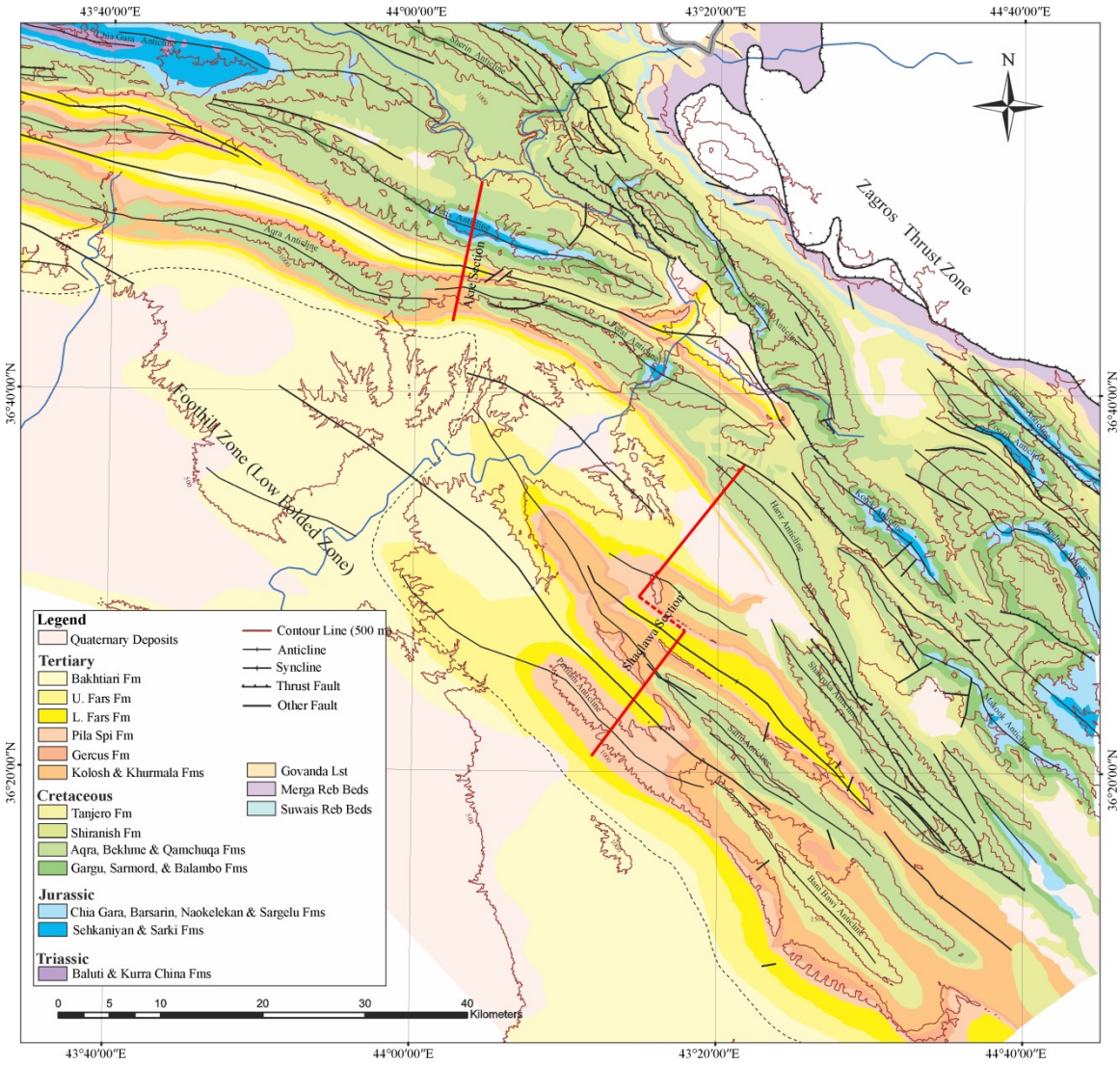

Figure 4-1: Geological map of the area reconstructed after Sissakian (1997) using field data and satellite image.

Folds in the area are primarily associated with thrusts (Omar, 2005; Jassim and Goff, 2006; De Vera et al., 2009; sections 2.6 and 4.5). Along the measured sections, folds are wide to broad and box-shaped. Based on Fleuty's (1964) classification of folds (using interlimb angles, which are calculated from the field data), folds have close to gentle inter-limb angles (Table 4-1; Figures 4-2 and 4-3). These classifications may vary along strike, especially in the Shaqlawa Section. The folds are spaced at wavelengths of 5

to 10 km with hinge lines varying from 25 to 70 km. Some associated thrusts cut all sedimentary units emerge at the surface while some remain blind thrusts. Two observed emergent thrusts include one in the southern limb of the Akre and Perat Anticlines and one in the southwestern limb of the Harir Anticline. Along sections, other folds are expected to be associated with thrusts based on interpreted seismic lines in the adjacent anticlines and geomorphic investigations (chapter 4). In addition, out-of-the syncline thrusts were observed in the northern limb of the Akre Anticline.

Table 4-1: Average dip for backlimb and forelimb, interlimb angle and classification (Fleuty, 1964) of anticlines in the measured sections.

Section	Anticline	Backlimb	Forelimb	Interlimb Angle	Fold Type
Shaqlawa	Harir	13	22	145	Gentle
	Khatibian	34	23	123	Gentle
	Safin	47	28	105	Open
	Pirmam	13	14	152	Gentle
Akre	Peris	77	60	43	Close
	Perat	46	58	76	Open

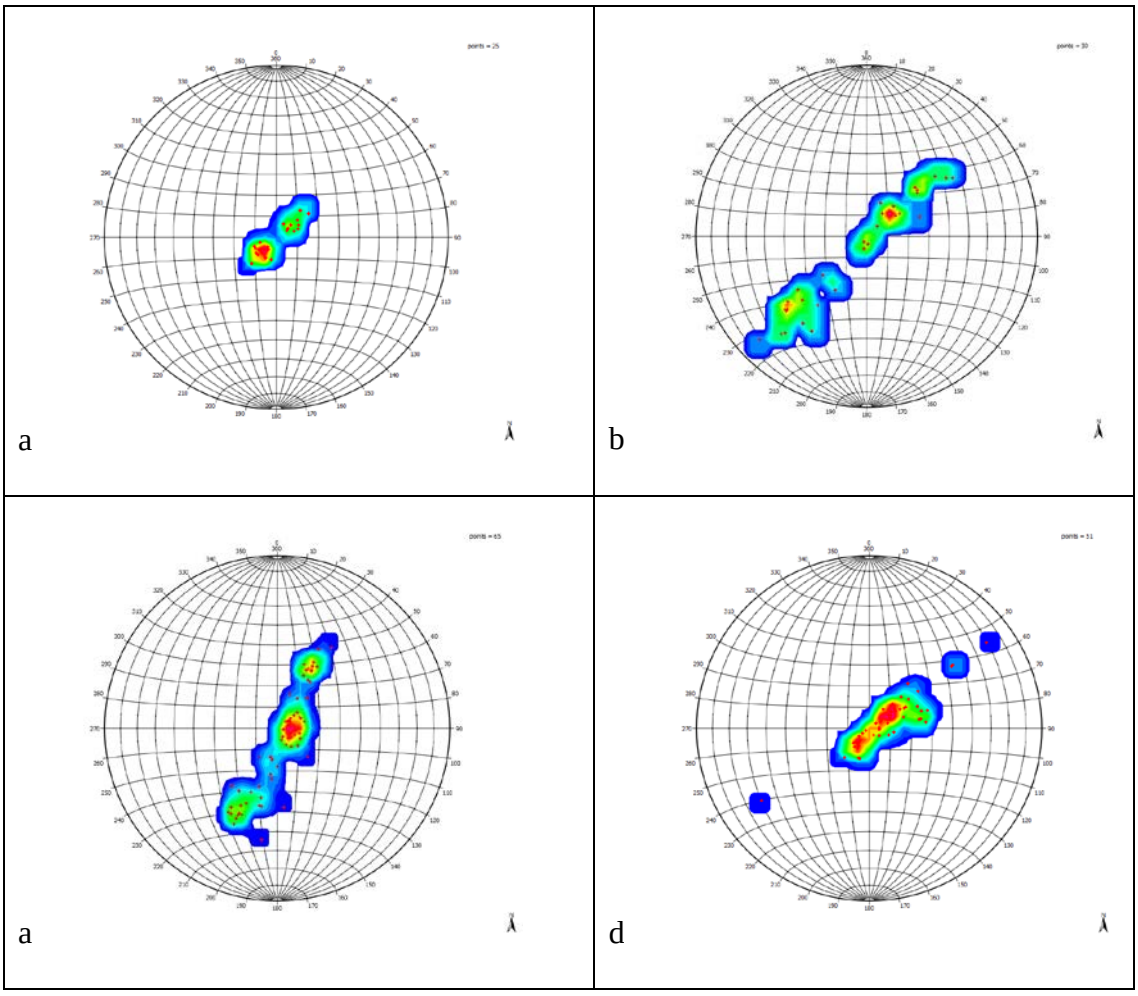

Figure 4-2: Stereographic projections of pole of planes along Shaqlawa sections; a) Pirmam, b) Safin, c) Khatibian, and d) Harir Anticlines

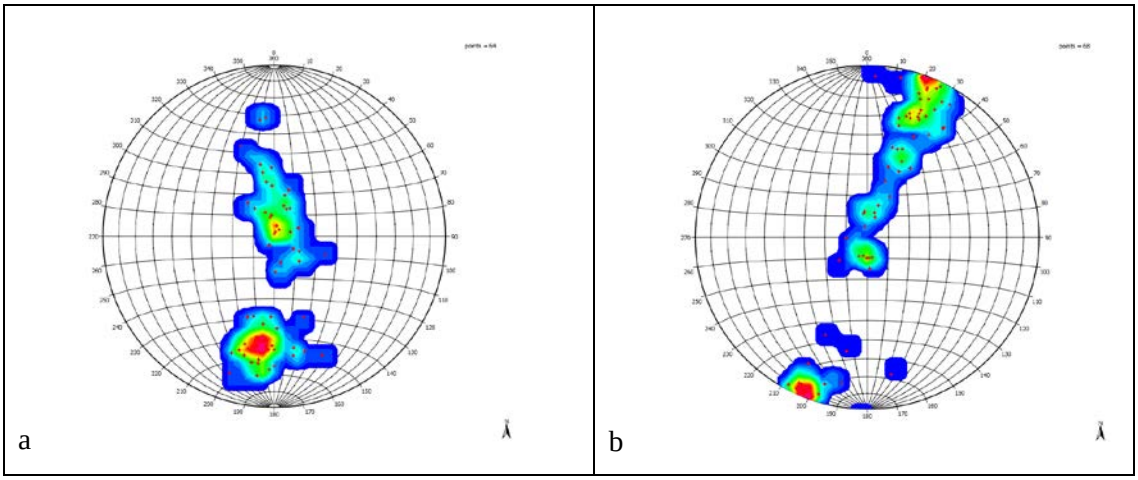

Figure 4-3: Stereographic projections of pole of planes along Akre sections a) Perat, and b) Peris Anticlines.

4.3 Depth to the Detachments

The calculated depths for detachment using area balancing method are 5.5 km or greater for Shaqlawa Section and 4 km or greater for Akre Section. Based on these values, the detachment is located within Triassic or older units. This method does not account for the presence of thrusts, thus is only an estimate depth to the detachment.

4.4 Balanced Cross-Sections

As useful tools to test the validity of the structural geometry of folds and faults described on cross-sections, balanced cross-sections were constructed along two sections. Fault geometry, bed length and cross-sectional area must be cautiously considered in construction of the balanced sections. In depth, faults are drawn based on available seismic lines, geomorphic indices of folds and the location of angular hinge regions in the section profile.

Displacement along the thrusts dies out to fault tips. This deformation gradient is not apparent in the emergent thrusts, but is observed in blind thrust. The variation in slip between footwall and hanging-wall cutoffs occurs mostly in incompetent units (e.g., shales and evaporites). The change in displacement magnitude along the thrusts may be due to simple shear along bedding plane of incompetent layers, intersection of the thrust with another thrust, or partitioning of strain between the thrust and other structures such as folds or cleavage (Marshak and Woodward, 1988).

4.4.1 Shaqlawa Section

In the Shaqlawa Section (Figure 4-4), the field observations in this study, which are consistent with those in a study by Omar (2005), suggest presence of an emergent

thrusts in the southeastern limb of the Harir Anticline. In the southwestern limb of the Harir Anticline, overturned beds occurred within the Shiranish Formation and for a short distance along the section. The overturned beds locate in between normally dipping units. The thrust is placed on the section to be coinciding with the location of the overturned beds. The high aspect ratio of the Safin Anticline (13.7; section 4.5) suggests that it is fault-related. Thrusts, which are placed on both Khatibian and Safin Anticlines are extrapolated from an interpreted seismic line (Csontos, et al., 2012; their figure 17) that is located about 15 km west of the current section. In the Khatibian Anticline thrusts occur in both limbs while in the Safin Anticline a thrust is present in its southwestern limb.

Displacement along the thrust in the southwestern limb of the Harir Anticline, which is measured as the dip separating of the footwall and hanging wall cutoffs, assuming constant thickness, is about 700 m. Other faults are blind and were shown in sections based on analogy with the seismic line, geomorphic indices of folds, and the location of hinge regions within the section. The displacement along blind thrusts is estimated at approximately 350 m along the thrust in the forelimb of the Safin Anticline and about 100 m along thrusts in both the forelimb and back limb of the Khatibian Anticline for the top Triassic horizon.

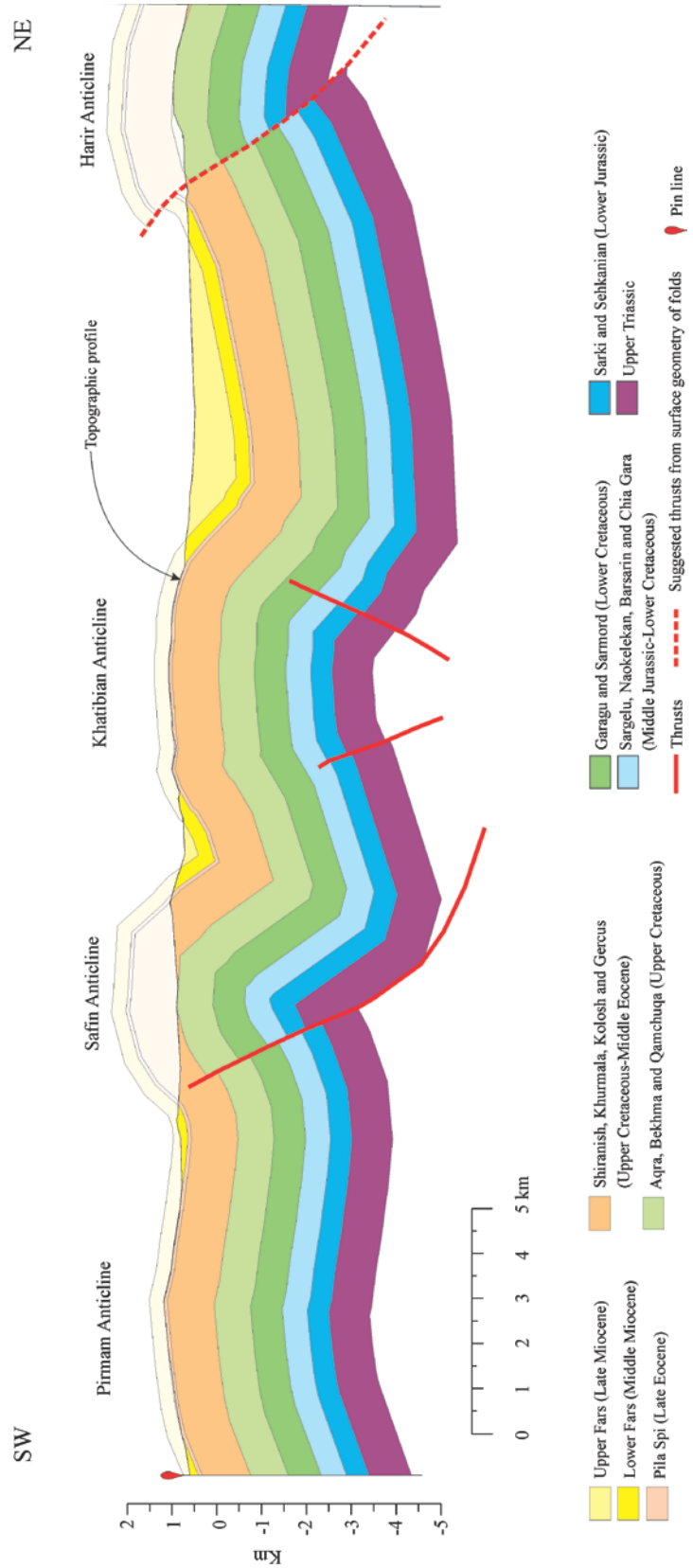

Figure 4-4: Structural cross-section in the Shaqlawa area.

4.4.2 Akre Section

In the Akre Section (figure 4-5), a thrust in the southern limb of the Perat Anticline is emergent based on the field observations and a study by Csontos et al. (2012). The geometry of the thrust and offset of stratigraphic units along it are extrapolated from a seismic line (Fogarasi, 2012). This thrust is considered the boundary between the High Folded Zone to the north and Foothill Zone to the south (jassim and Goff, 2006). The aspect ratio of the Peris Anticline is about 10.7 (Section 4.5) and this suggests that it is also fault-related. Thrusts in both limbs of the anticline are placed based on the location of hinge regions in the section profile. In general, blind thrusts (i.e., their ramps) are drawn to be sub-parallel to the dip of the opposite limb.

Displacement along the fault in the southern limb of the Perat Anticline near its western tip close to linkage area with the Akre Anticline as measured from seismic data (Fogarasi, 2012) is approximately 2500 m. Other thrusts in the section are blind. The displacement of thrusts in both forelimb and backlimb of the Peris Anticline is estimated from the cross-section (Figure 4-5) at approximately 150 m for the top Triassic horizon.

The folding dies out down-section in the core of Peris Anticline when they reach horizons within the Triassic units by adding horizons down-section. If additional horizons are added below and parallel to the Triassic units, they become less folded in comparison to those that are located above. This also supports having a possible detachment level within the Triassic units.

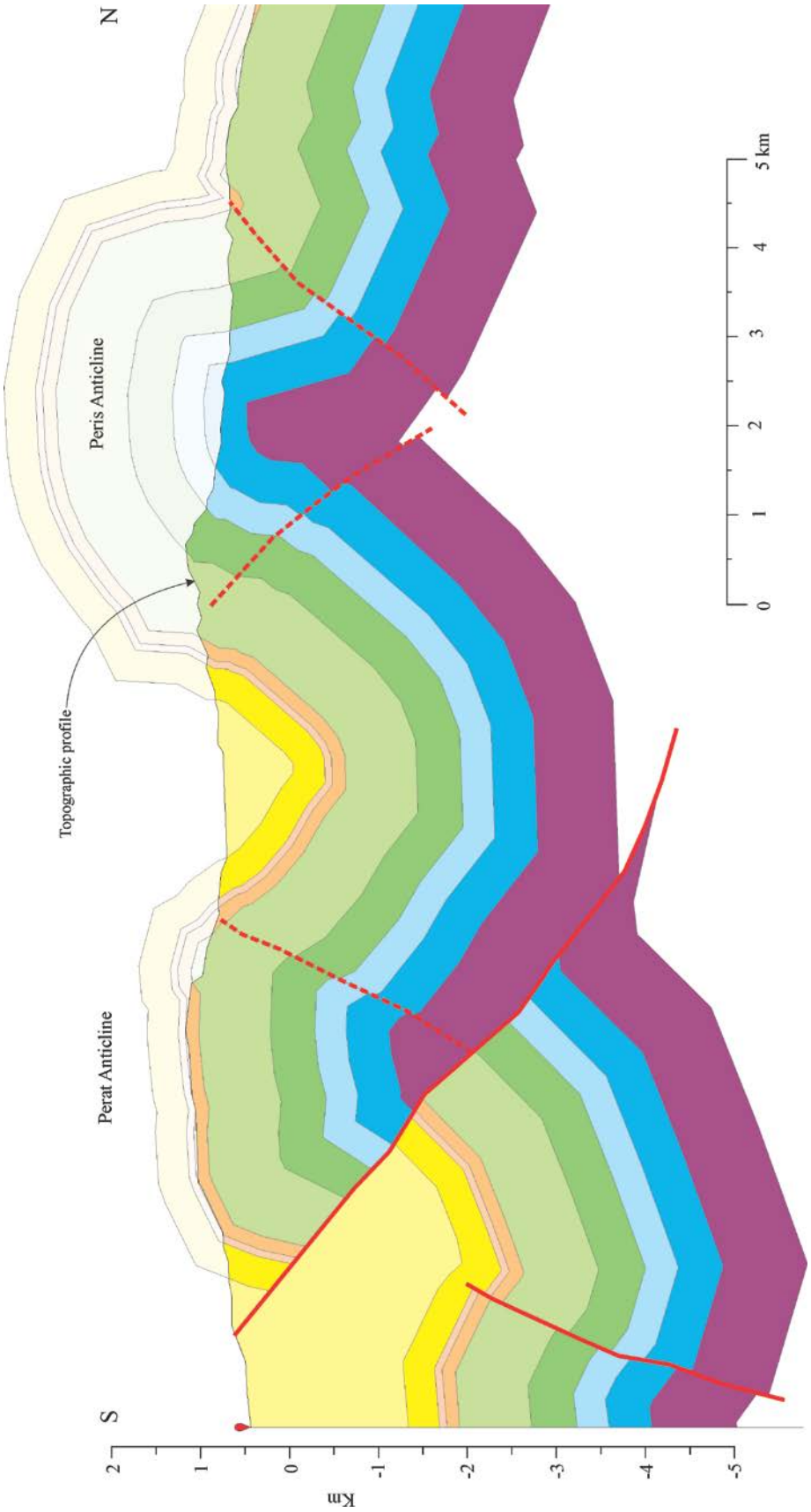

Figure 4-5: Structural cross-section in the Akre area (note: the legend is the same as in Figure 4-4).

4.5 Comparison to Seismic Data

The structures that are placed on cross-sections were compared with those that are present on publicly available seismic lines, to verify these structures, except those that are placed in the Peris Anticline because there is no available seismic line across the anticline. In seismic lines (Figures 4-6 and 4-7), folds are associated with thrusts of relatively steep dip. The constructed horizons in the cross-sections are more angular than those in the seismic lines because the dip data were divided to a number of domains with fairly close dip amounts in sections (the kink band method). Thrusts may dip N- or NE-ward (consistent with the direction of the deformation propagation) or may dip S-or SW-ward (opposite to the direction of the deformation propagation).

One of the available seismic lines is located across the eastern portion of the Perat Anticline (Figure 4-6). The fold is open with a broad crest area. It is a whaleback-shaped anticline covered by Upper Cretaceous carbonates. The northern limb of the anticline is steeper than the southern limb. The main thrust is dipping south-ward. There is a back thrust (antithetic thrust) dipping north-ward which is being intersected by another synthetic thrust that is parallel to the main thrust. In this seismic line, there is a thickening in the Jurassic units in the core of the anticline. This may be due to the presence of weaker units possibly containing shale and/or evaporites.

A second seismic line runs across the Shakrok Anticline (Figure 4-7) which is broad with a steeper southwestern limb. In addition to the main fold, secondary folding occurs in the fold crest. A small syncline was formed in the crest and separates it into two synclines. The main thrust is steep, dips northeast and cross-cuts the southwestern limb. An oblique slip fault with relatively low displacement cross-cuts the northern limb. Strike

slip movement is detected along normal faults that occur in the northern limb of the Shakrok Anticline (Omar, 2005).

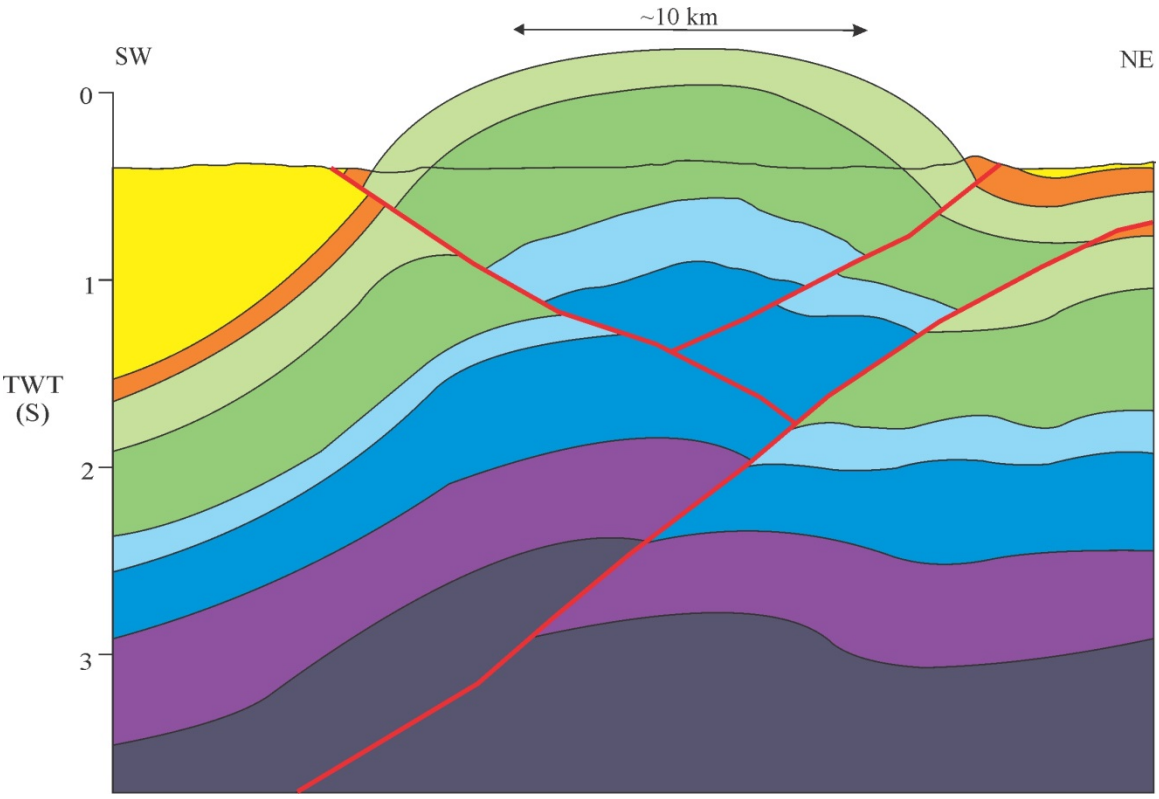

Figure 4-6: Interpreted seismic line across the eastern side of the Perat Anticline in Bekhme. The main thrust is dipping southwest (note: the legend is the same as in Figure 4-4); seismic line is from Fogarasi, 2012).

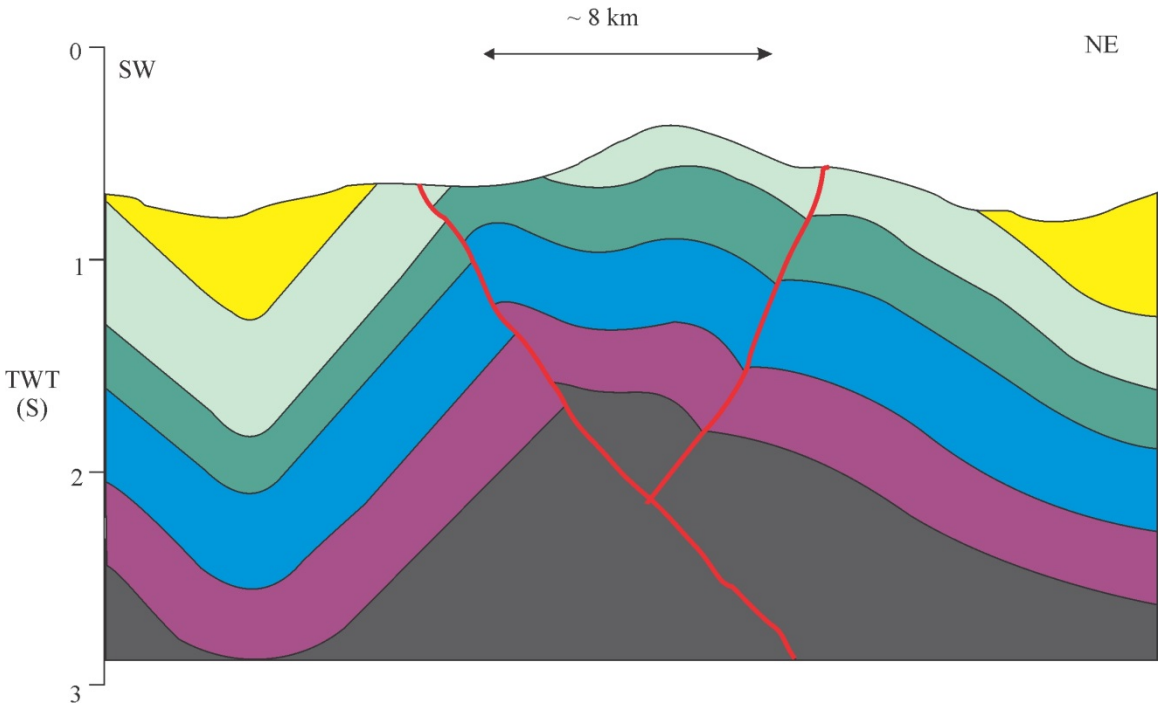

Figure 4-7: Interpreted seismic line across the western side of the Shakrok Anticline. The main thrust is dipping northeast-ward (note: the legend is the same as in Figure 4-4); seismic line is from Petroceltic, 2013).

4.6 Restored Sections

Cross-sections were restored using the line length and area balancing methods. Sections were restored maintaining the original length of the horizons and maintaining the area of geologic units in the sections. The pin lines were positioned in the southern end of section because the strata in these locations are slightly tilted and they are not too much different from the regional dip. Loose lines were placed in the trailing edge of section in their northern end. After restoring the cross-section, the shortening along the sections was measured.

4.6.1 Shaqlawa Section

The shortening was measured at 12 % along the Shaqlawa Section. Relatively low shortening in Shaqlawa is due to the location of the section, which is located in the western side of the folds close to their plunging area. Consequently, the shortening is expected to be higher in sections close to the central part of folds further to the east of the current section. This trend was selected because it was the best accessible trend across the folds in the eastern segment for collecting field data.

The restored loose line at the trailing end of the Shaqlawa Section is straight (Figure 4-8). The straight loose line is considered admissible (Marshak and Woodward, 1988). Thus, there is minimal variation in shortening between horizons in this section. Geometry of thrusts after restoring shows gradually curved lines. The curve becomes gentler when it cut down through the Triassic units (e. g. in the Safin Anticline). This is also admissible situation.

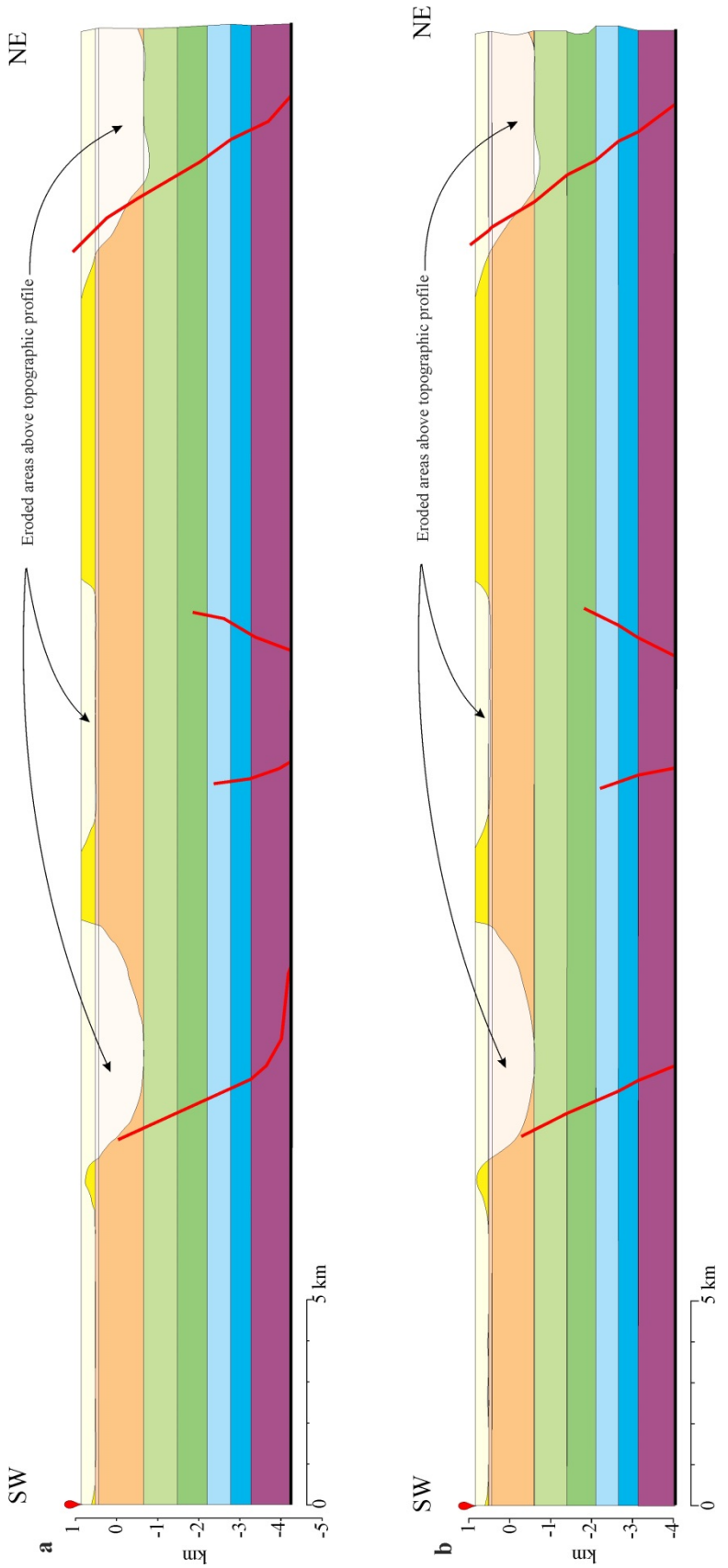

Figure 4-8: Restored cross-section of Shaqlawa area, a) using line length method and b) using area balancing methods (note: the legend is the same as in Figure 4-4).

4.6.2 Akre Section

After restoring the cross-section, the shortening along the section was measured. The shortening was measured at 20 to 29 % along the Akre Section. The shortening in the Akre Section varies because the horizons become less folded toward the core of anticlines due to concentric folding (e.g. in the Peris Anticline). The upper horizons accommodate more shortening than the lower horizons due to concentric folding. In addition, the Triassic units are considered to be the detachment. Shortening is observed to vary between horizons that are separated by detachment (Dahlstrom, 1969; Woodward et al., 1989).

In the Akre Section, the restored loose line is slightly curving from Upper Cretaceous to Upper Triassic horizons (Figure 4-9). To this point it is considered as admissible. From an Upper Triassic horizon to a horizon within the Triassic, the loose line is more stepped and this is not admissible. This step in the loose line is due to the decrease of folding toward the core of the anticlines. The horizon within the Triassic accommodates less shortening than the Upper Triassic horizon. In the line length balancing, these kind of problems appear when to horizons are separated by a detachment (Woodward et al., 1989). In such cases, more data are needed to resolve this kind of contradictions. In the restored section, geometry of thrusts after restoring shows gradually curved lines. The curve becomes gentler when it cut down through the Triassic units. This is also admissible situation.

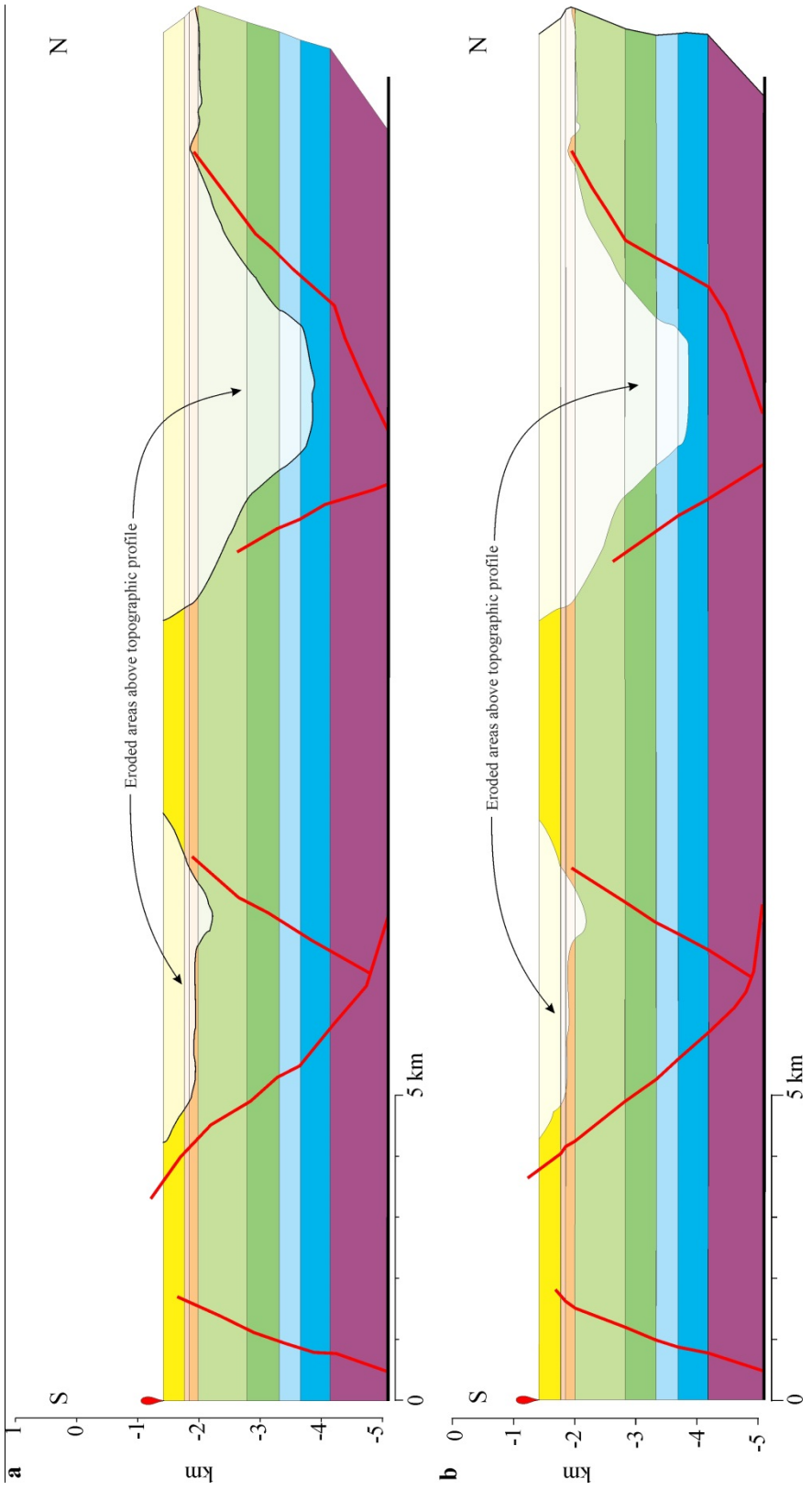

Figure 4-9: Restored cross-section of area using a) line length balancing method, and b) using area balancing method(note: the legend is the same as in Figure 4-4).

4.7 Along Strike Variations

Variations are expected to be present along strike of one specific fold. These variations may be present in the geometry of the fold itself or associated faults. These changes are reflected in the attitude of the fold limbs and the geomorphology of the fold. Generally, the limb that accommodates the main thrust is steeper. This feature can be evidenced in folds in the constructed cross-sections and interpreted seismic lines (Figures from 4-4 to 4-7). One exception is the Safin Anticline (Figure 4-4) where the main thrust is dipping northwest and the northwest limb (back limb) is steeper.

A noticeable example of variation along strike is the Perat Anticline. The main thrust of the Perat Anticline in the eastern side is dipping south-ward as it is shown in the seismic line (Figure 4-6), while in the western side the main thrust is dipping north-ward as it is shown in the Akre Section (Figure 4-5), indicating variation in the main thrust along strike. This suggests that the anticline is located above the linkage of two faults. However, there is little pronounced geomorphological indication of linkage along it. It is widening toward the east and there is a change in hinge line direction along the fold crest. In addition, the slope as it shown from topographic profiles across the fold is steeper in the northern limb in the eastern side and steeper in the southern limb in the western side (Figure 4-10). This change in the slope along the fold matches with the dip direction of the main thrust.

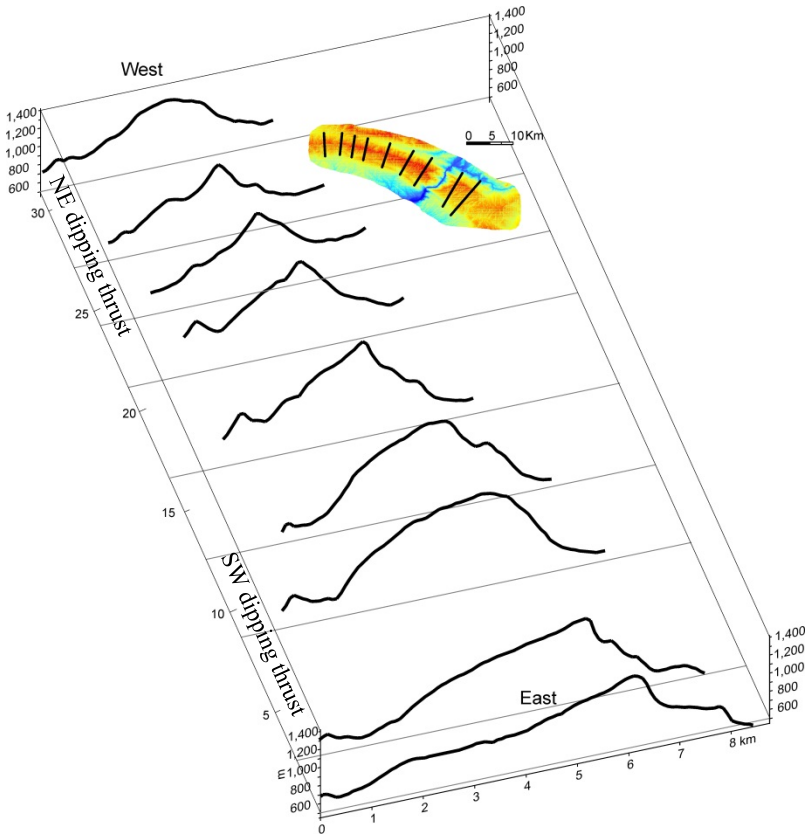

Figure 4-10: variations in the topographic profiles across Perat Anticline; in the eastern part (where the thrust is dipping SW), the northern limb is much steeper than the southern limb, toward the west (where thrust is dipping NE) slope of northern limb decreases. These indicate lateral variation along the fold.

4.8 Fold-Accommodation Thrusts

A number of smaller scale thrusts were also detected in the northern limb of the Akre Anticline. These thrusts dip toward the north with displacement of ~10 m (Figure 4-11). The thrusts are interpreted as fold-accommodation thrusts. These faults extend from the Dinarta Syncline to its southern limb (forelimb), which is gentler than the northern limb. Thus, they are considered to be out-of-syncline faults. This type of fault is also detected in the Iranian Zagros (Fard et al., 2006; Alavi, 2007). Out-of-the syncline thrusts are considered to be secondary structures that accommodate strain discontinuities during folding. These folds form due to increase in bed curvature within syncline cores, with differential layer-parallel strain also contributing to thrust slip (Mitra, 2002). Due to

relatively low displacement (~10 m) along these faults, they are not included during the construction of these cross-sections.

c

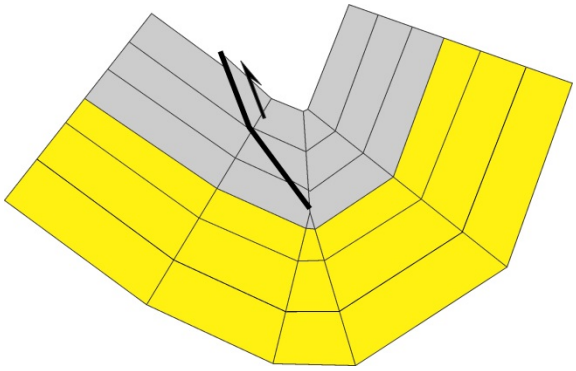

Figure 4-11: a, b) Out-of-syncline thrusts with low displacement in northern limb of Akre Anticline; c) diagram of out-of-syncline thrust (Mitra, 2002).

5-RESULTS: GEOMORPHIC CRITERIA THAT INDICATE FOLD GROWTH

5.1 Introduction

In tectonically active regions (e.g. fold-thrust belts), folds grow in three dimensions by fold uplift, limb rotation and lateral growth (Azor et al., 2002). In these regions, the landscape that is developed is the function of erosion and/or deposition as well as the growth of active structures (Jackson et al., 1996). In these regions, the tectonic activities are represented by the development of fault-related folds. The geomorphic features of these folds may reveal information about the direction and rates of lateral propagation of faults and related folds (Keller et al., 1999). In addition the 3D geometry including the aspect ratio and symmetry index of folds may disclose the relationship between the folds and related faults (Cosgrove and Ameen, 2000; Blanc et al., 2003; Burberry et al., 2010). This chapter deals mainly with the geomorphic features such as drainage networks, wind and water gaps, fold front sinuosity and the topographic profile along the fold crests that may indicate lateral growth of folds and relative age of folds and geomorphic indices such as aspect ratio and fold symmetry index that may help categorizing fault-related folds in the area.

5.2 Folding Age and Geomorphic Criteria Preservation

The convergence in the Zagros Fold-Thrust Belt may have started in the Early Miocene and propagated SW during the Pliocene (Hessami et al., 2001; Csontos et al., 2012). In the Lorestan Provence, Iran, the main folding occurred in the Middle-Late Miocene (Navabpour et al., 2008). It is expected to be coeval with the folding in the Iraqi

Zagros. The NW segment of the Zagros Fold-Thrust Belt (Kirkuk Embayment) is located within the Middle Miocene-Pliocene convergence zone, and the youngest geologic unit (the Upper Miocene-Pliocene Bakhtiari Group) is affected by folding (Csontos et al., 2012).

The folding in the NW segment of the Zagros Fold-Thrust Belt in N Iraq including the study area started during the Middle Miocene-Pliocene. From that time, a number of superimposed tectonic and geomorphic events may have occurred based on successive pulses of folding. The younger events probably overprint the older ones, as well as the geomorphic features. In addition, during the evolution of the Zagros Fold-Thrust Belt, the whole Cenozoic sedimentary cover (2-3 km thick) has been removed by erosion in some anticlines. However, Bretis et al. (2011) and Ramsey et al. (2008) detected direct geomorphic evidence of lateral growth of folds in the Safin, Bani Bawi and Pirmam Anticlines in the study area and in the Zagros Simply Folded Belt in the Fars Provence, Iran, respectively.

5.3 Geomorphic Criteria

In this segment of the Zagros Fold-Thrust Belt, a number of criteria that may indicate growth of folds can be noted. Using only one geomorphic criterion to indicate fold type and growth may lead to error in results. Thus, using a number of geomorphic criteria is recommended in order to obtain reliable results (Burbank and Anderson, 2012). DEMs that were extracted from the SRTM datasets were used to construct a topographic map, a stream network map, and terrain profiles along the fold crests. The maps and fold crest profiles were used to understand the morphological criteria and landscape evolution that resulting from the fold evolution. The geomorphic criteria that are used to understand

fold evolution include drainage network, wind and water gaps, topographic profile along fold crest and fold front sinuosity.

5.3.1 Drainage Network

The typical drainage network of the Zagros Fold-Thrust Belt is primarily made up of fan- shaped tributary patterns on the flanks of the whaleback folds (Ramsey et al., 2008). In the study area, the fan- shaped tributary patterns are detected on folds that expose the Upper Cretaceous carbonates (Aqra and Bekhme formations) and Pila Spi limestone. Analysis of these tributaries may be used as an indicator of fold evolution.

Distinctive asymmetric forked tributary patterns have developed to the direction of fold propagation in the study area (Figure 5-1). In the fold noses, tributaries run sub-parallel to fold hinge. When a fold grows laterally, the tributaries in the fold flanks (which were previously in the fold nose) track toward the growth direction instead of following the steepest topographic gradient perpendicular to the contour lines (Figure 5-2).

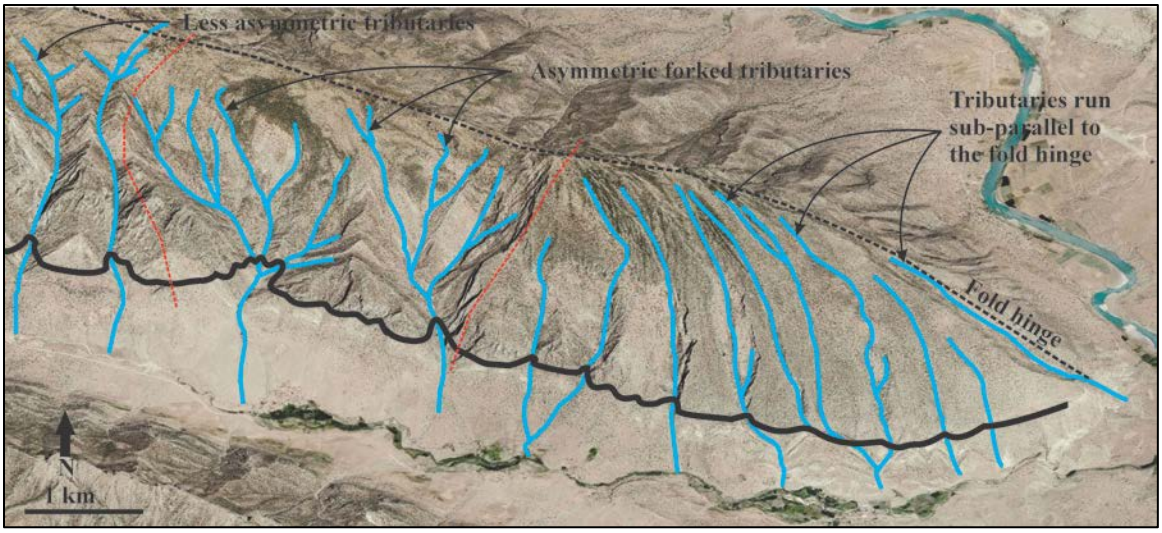

Figure 5-1: Developments of tributary (blue) in response to lateral growth of fold and fold front sinuosity (black); eastern end of Peris Anticline. In the plunging end, the tributaries follow the slope and run somewhat parallel to the fold axis. Toward the center of fold, tributaries become more dendritic, but still preserve the original direction to some degrees and the fold front become less sinuous toward the plunge area (image is from Bing Map).

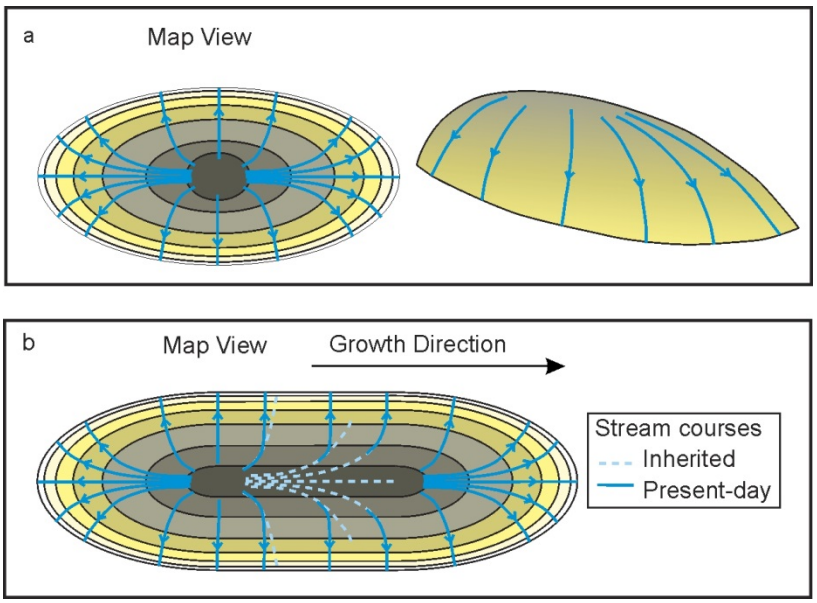

Figure 5-2: (a) Tributary pattern for a typical plunging whaleback fold (b) The tributary pattern for the same fold in that has grown in laterally to the right (Ramsey et al., 2008).

In the northwestern half of the Harir Anticline, which is covered by the Upper Cretaceous Bekhme Limestone and has a whale-back shape, the tributaries flow west-ward parallel to the fold axis on the crest of the anticline (Figure 5-3), especially in the

forelimb. These tributaries are asymmetrical and forked in shape. This style is developed from the pre-existing tributaries in the fold nose that runs parallel to the fold axis. With the propagation of hinge line northwest-ward, the new drainage network on the fold crest is inherited from the one in the fold nose. With the time and rotation of fold limbs, the hinge regions have been uplifted. When these tributaries pass the hinge regions down to the steepest parts of fold limb, they track the steepest topographic gradient perpendicular to the fold axis in parallel patterns. In these parts, the tributaries were not affected by the pre-existing tributaries in the plunge area. The same style of tributaries is present in the northwestern side of the Shakrok and Safin Anticlines (Figures 5-4). In other anticlines this style of tributaries can be seen only in areas close to the fold nose. Asymmetric forked tributaries exist in areas close to the fold noses, and in the fold tip they run parallel to the hinge line (Figure 5-1).

The asymmetric forked tributary style in northwestern half of Harir, Shakrok and Safin Anticlines suggests that these folds have propagated northwest-ward. The asymmetric forked tributary style in the fold nose of the other anticlines does not disclose information about their lateral growth. This type of tributary style is typical in the fold noses even without lateral growth.

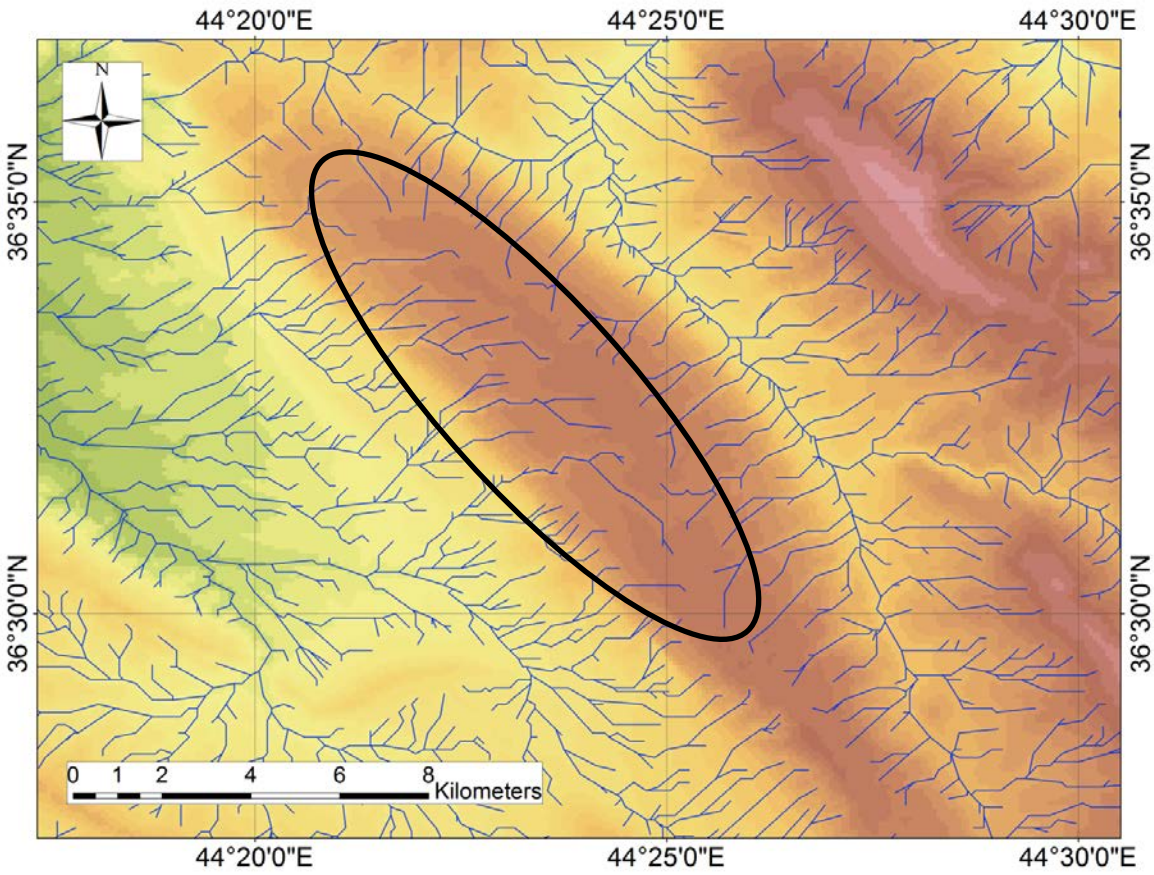

Figure 5-3: Tributaries in the Harir Anticline; Tributaries are in asymmetrical forked-shape running parallel to the fold axis on the crest northwest-ward and then fallen down the fold flanks, which suggest northwest-ward growth of the fold.

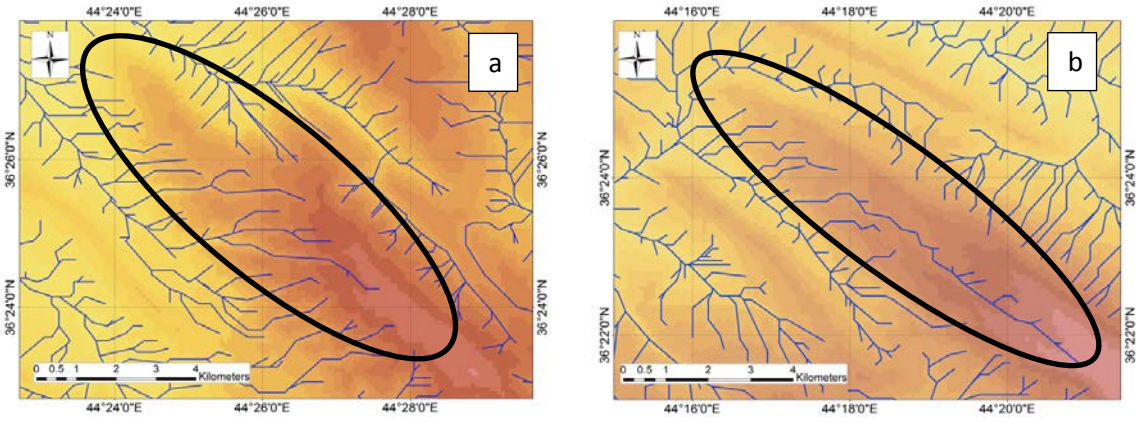

Figure 5-4: Tributary patterns in the western side of Shakrok Anticline (a) and in the western side of Safin Anticline (b), suggesting northwest-ward propagation of these folds.

5.3.2 Water and Wind Gaps

A number of wind and water gaps, which may also indicate lateral growth of folds, have developed in this area. Rivers have been diverted around the tip of folds whenever uplift rates higher then downcutting (erosion) rates by the rivers across folds (Figure 5-5). Water and wind gaps are present in Harir, Safin and Aqra Anticlines. In Harir Anticline, there are two wind gaps and one water gap at its western side within a distance of 3.5 km (Figure 5-6). These gaps were formed from the diversion of a single stream. The two wind gaps are located to the east of the water gap. With the west-ward growth of the fold, the stream was diverted around the fold tip leaving abandoned stream as the first wind gap, and so on to form the second wind gap. The elevations of water and wind gaps decrease to the northwest side of the fold. In Aqra Anticline, there is a wind gap located at the western side of the fold at a distance 13.2 km from current stream or water gap (Figure 5-7a). With the uplifting of the fold the streams have been diverted from their original paths (approximately straight) and bent around the tip of the fold to pinch between tips of two anticlines. In Safin Anticline, a stream that made the wind gap cannot be traced on the map (Figure 5-7b). The wind gap is only indicated from the topography of the anticline crest. Thus, this gap cannot be used to indicate direction of lateral propagation of the fold itself.

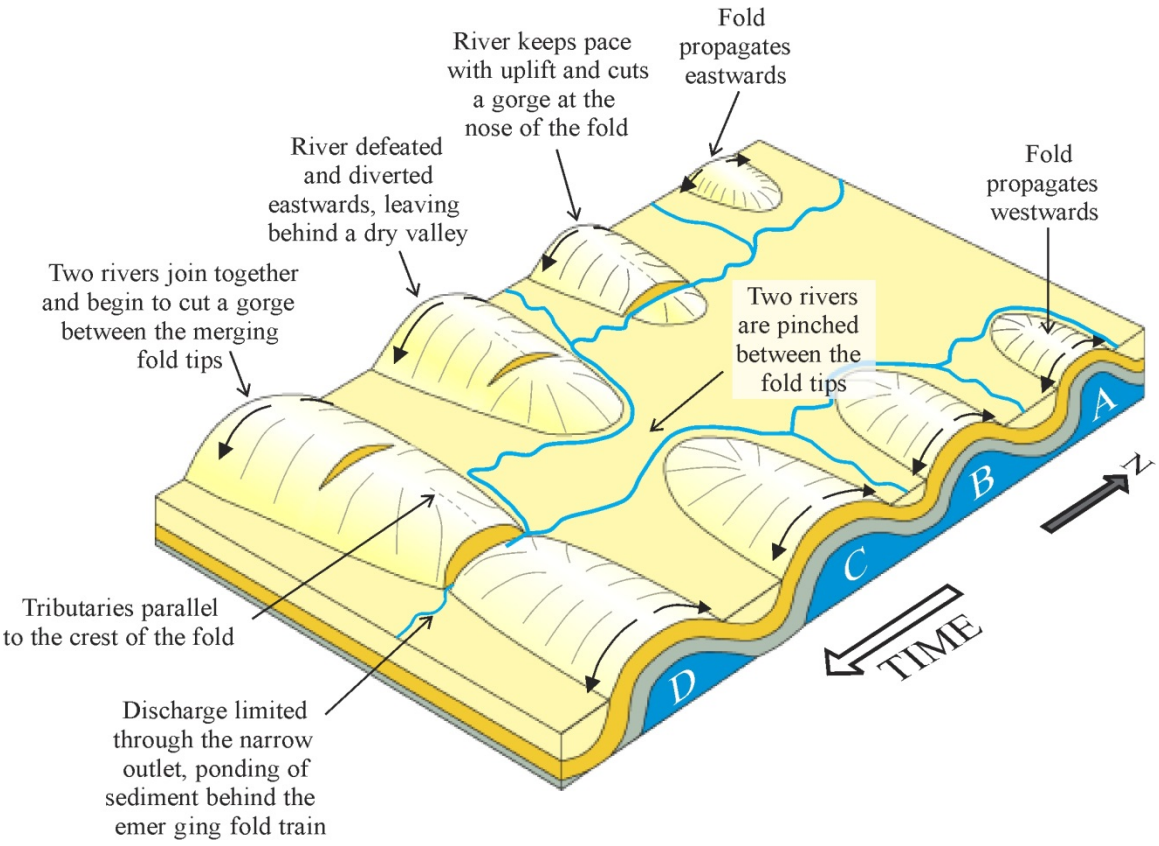

Figure 5-5: Cartoon showing formation of water and wind gaps by running streams in the laterally growing folds from stages A to D (Ramsey et al., 2008).

Throughout the wind and water gaps that occur in this area, the lateral growth can be indicated only in the Harir Anticline due to presence of two wind gaps followed by a water gap. Formation of a series of wind gaps by one stream is the strongest indicator of lateral growth of folds (Ramsey et al., 2008). In fixed-length folds, which do not propagate laterally, streams may divert only one time around the fold nose leaving only one wind gap. In laterally propagated folds, streams may divert more than one time around the fold nose leaving a series of wind gaps along the fold crest (Ramsey et al., 2008). Consequently, the presence of a water gap and only one wind gap cannot necessarily indicate lateral migration, because the stream has been diverted by uplift of the fold, but there is no evidence of gradual propagation of the fold toward the water gap

side. Thus, the water and wind gaps in the Safin and Aqra Anticlines cannot reliably be used as indicators of fold lateral growth.

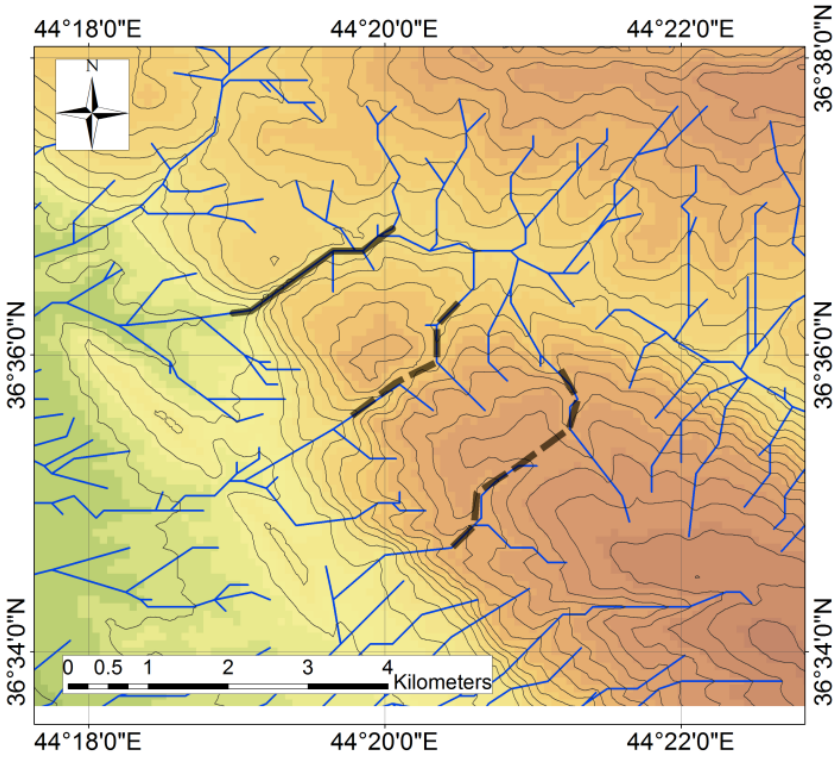

Figure 5-6: Wind gaps (dashed black line) and water gaps (solid black line) in western side of Harir Anticline.

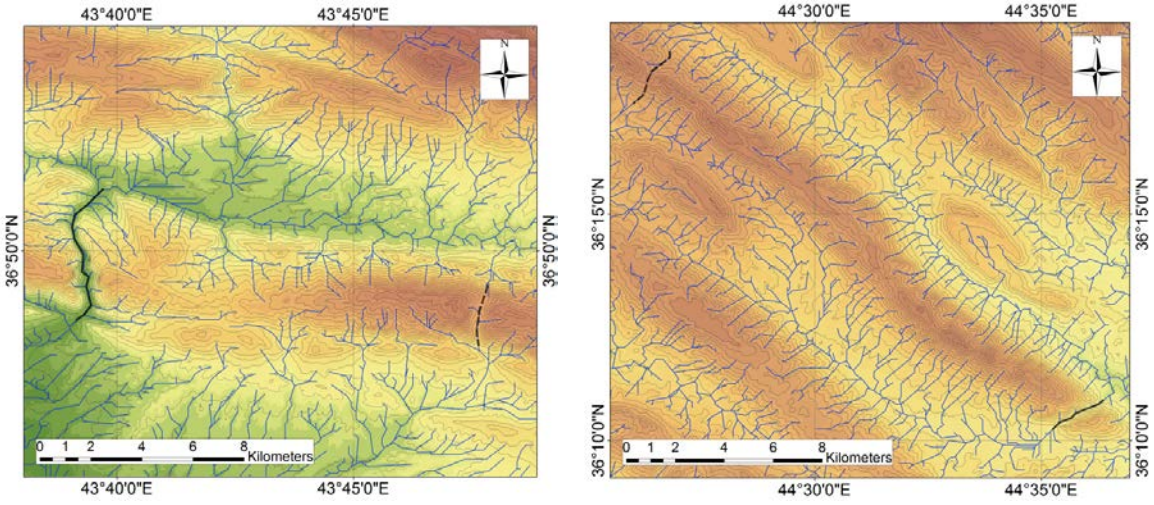

Figure 5-7: Wind gaps (dashed black line) and water gaps (solid black line) at a) western side of Aqra Anticline and b) eastern side of Safin Anticline.

5.3.3 Long Topographic Profile along Fold Crest

The long topographic profiles along the fold crests parallel to their hinge line were constructed from DEMs (Figure 5-8). Based on variations in the profile and exposed lithology along the fold crests, folds can be divided into two groups. The first group shows few variations through their long topographic profiles, except in incised valleys by main streams and in fold noses. The exposed rocks along the crest of these folds are mostly composed of Upper Cretaceous carbonate. This group includes Aqra, Perat, Peris and Harir Anticlines. The first three anticlines are located in the western side of the study area. The second group shows variations along their topographic profiles. The exposed lithology varies from the Upper Cretaceous carbonates to Upper Cretaceous and Tertiary clastics to Eocene carbonate (Pila Spi Formation). This group includes Pirmam/Bani Bawi, Safin and Shakrok/Khatibian anticlines. These are located in the eastern segment of the study area. In the Safin Anticline, the elevation is higher in the central part, while in Pirmam/Bani Bawi and Shakrok/Khatibian anticlines, it is higher in southwestern parts with respect to exposed rock units.

Northwest-ward decrease in relief of the long topographic profile along the crest of the Shakrok/Khatibian and Pirmam/Bani Bawi Anticlines with respect to the exposed stratigraphy may indicate northwest-ward propagation of these anticlines. In the Safin Anticline, the long topographic profile is decreasing in both northwest and southeast direction from the central part and this suggests that the anticline propagated from the central part (near Shaqlawa City) southeast-ward and northwest-ward.

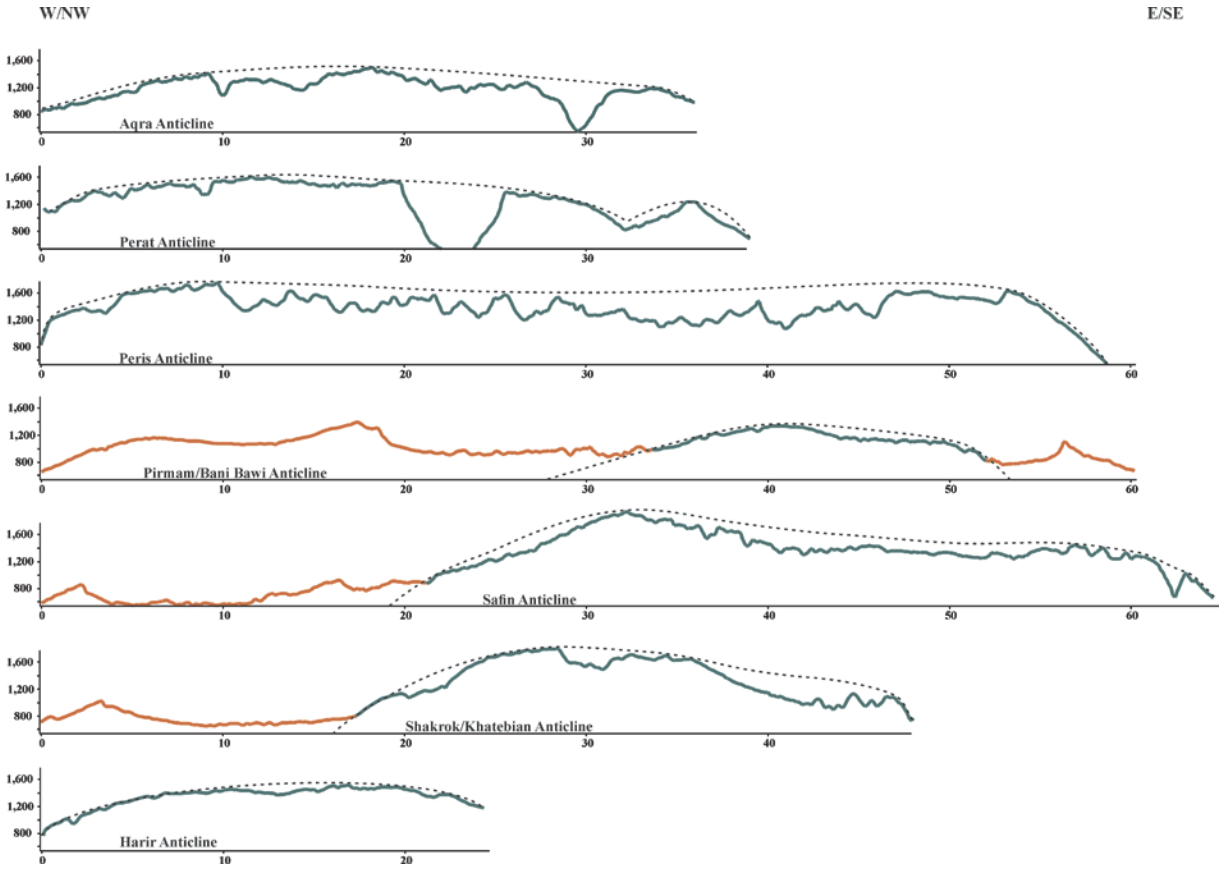

Figure 5-8: Long topographic profiles along the fold crest; red line represents areas where the Tertiary rocks are exposed, green line represents area where the Cretaceous carbonates rocks are exposed are exposed and dashed black line is the expected top of the Cretaceous carbonates without erosion.

5.3.4 Fold Front Sinuosity

In this part of the Zagros Fold-Thrust Belt, erosion cuts through the sedimentary units in to a fold front. In some folds (e. g. Pirmam Anticline) erosion cut through the Neogene units to stop by the resistant Pila Spi limestone. In other folds (especially older folds, which are located in the northeastern part of the area) erosion acted further through the Cenozoic formations to the Upper Cretaceous limestone.

Figure (5-9) shows the fold front sinuosity of folds in the area. In general, the fold front sinuosity increases northeast-ward. The folds that are closer to the backstop of the

Zagros Fold-Thrust Belt exhibit higher fold sinuosity index. The values of fold front sinuosity vary from 1.3 in the southwest folds to almost 2.0 in the in the northeast folds. Even within a single fold, fold front sinuosity may change from one segment to another. The southeastern half of the Shakrok Anticline exhibits higher fold front sinuosity than the northwestern halves. The southeastern end of the Harir Anticline also is more sinuous than other parts, as well as the central part of the Safin and Akre Anticlines. In other folds, such as Peris Anticline (Figure 5-1), the fold front sinuosity declines in areas close to their tips.

Since the deformation in the Zagros Fold-Thrust Belt propagated southwest-ward, the northeastern most folds were formed first and these folds were exposed to erosion for a longer time. Consequently, their fold fronts became more sinuous. Within a single fold, the segments that have been uplifted first have a higher fold front sinuosity higher than later uplifted segments. In the Shakrok and Harir Anticlines, increasing the fold front sinuosity southeast-ward suggests that the southeastern parts of these folds were uplifted first and exposed to the erosion for a longer time than the northwestern parts. Also higher fold front sinuosity in the central parts of the Safin and Akre Anticlines suggests that these parts were uplifted and exposed to the erosion first.

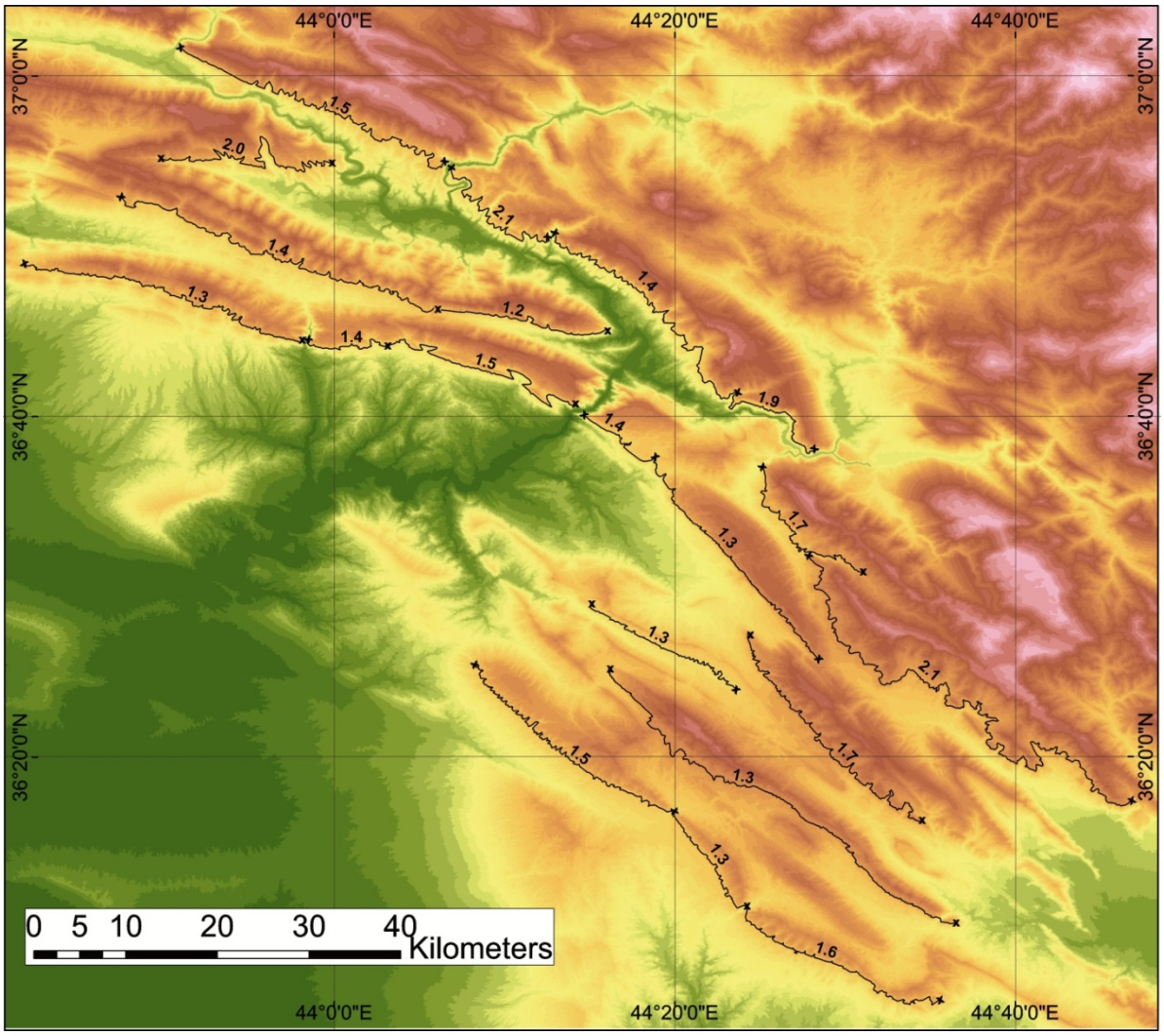

Figure 5-9: Fold front sinuosity (FFS) of the folds shown by number for each fold or fold segment (refer to the Figure 3-1 for fold names).

5.4 Lateral Growth of Folds and Fold Segments

By combining results from different geomorphic investigations that indicate lateral growth of folds, we can more confidently state that the Harir, Shakrok/Khatibian, Safin and Bani Bawi/Pirmam Anticlines have indeed propagated laterally (figure 5-10). Most of the geomorphic criteria indicate that these folds are growing northwest-ward. These folds are located in the eastern side of the study area. The folds in the western side,

which include Perat, Akre and Peris Anticlines, do not demonstrate indicators of lateral growth, except in parts close to the fold noses.

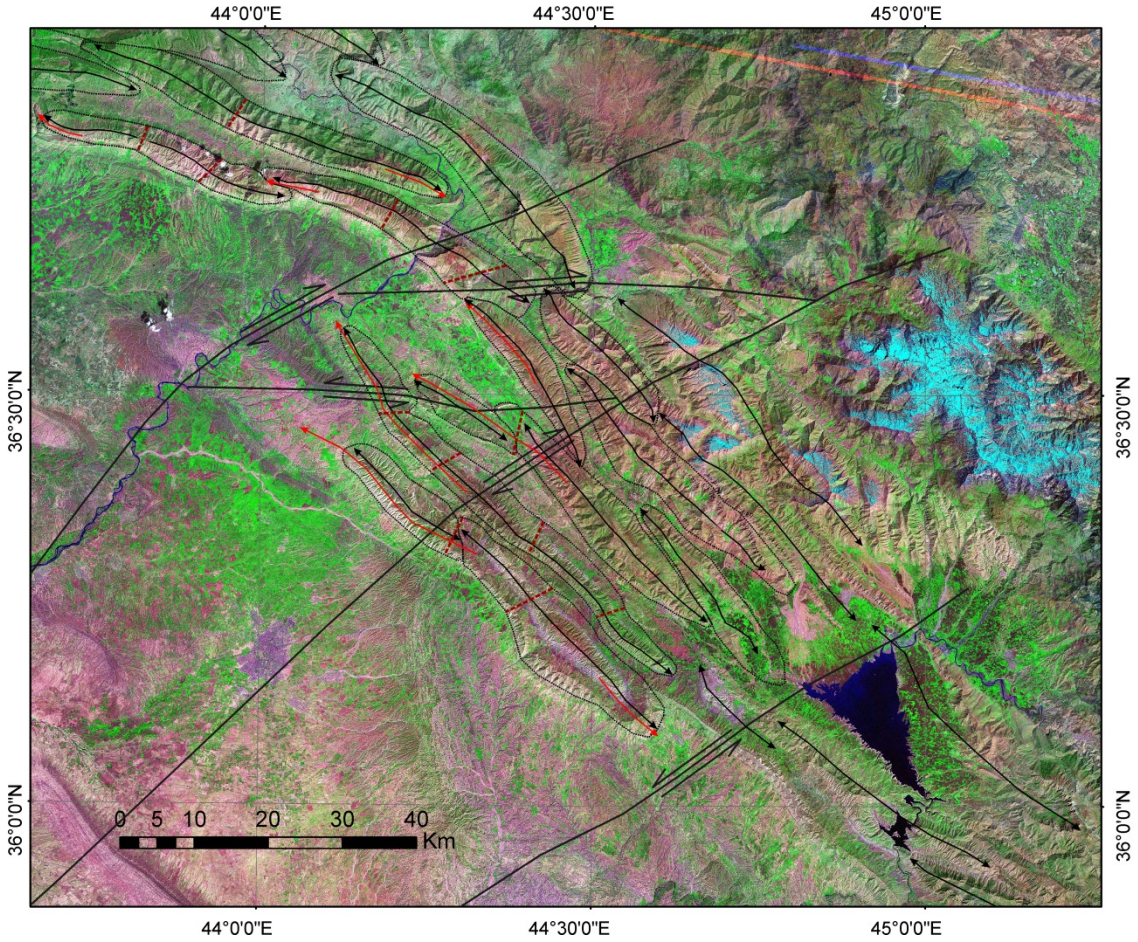

Figure 5-10: Map of folds in the area, showing fold segments, inclusive lateral propagation of folds (refer to the Figure 3-1 for fold names) and regional lineaments, which are interpreted as basement faults (lineaments are from Omar, 2005).

Based on geomorphology of the folds and direction of hinge lines, folds can be divided to number of segments (figure 5-10). These segments probably started as separate folds related to separate thrusts. Then, they propagated laterally with the evolution of deformation and linked to form one single linear fold or a series of closely spaced *en-echelon* structures. After linkage, the linked folds and their related thrusts begin to

overlap. The topography in the linkage area becomes smoother after a long time from linkage (Burbank et al., 1999). Thus, the geomorphic criteria that indicate lateral growth may progressively disappear. There are variations in the direction of hinge lines along the folds that display lateral growth. This indicates changes in the stress direction with the time.

5.5 Geomorphic Indices of Folds

The folds in this part of the Zagros Fold-Thrust Belt have been considered as a large-scale buckle folds by some authors (e.g. Sattarzadeh et al., 2000). Buckle folds form from shortening of layers parallel to the layering (Fossen, 2010). Buckle folds have periclinal geometry (i. e., folds that have the form of an elongate dome). These are usually described by an aspect ratio, which is calculated as the ratio of the fold hinge length to the width of fold or half wavelength (Cosgrove and Ameen, 2000). However, the presence of forced folds has been inferred from satellite images, and gravity in the Kirkuk Embayment (Ameen, 1991). Aspect ratio of the buckle folds ranges between 5 and 10, while forced folds have an aspect ratio of more than 10 (Sattarzadeh et al., 2000; Blanc et al., 2003). As a function of the stratigraphy, depth and regional tectonic setting, detachment folds, fault-propagation folds and fault- bend folds have developed in the Zagros Fold-Thrust Belt in Iran and in the NW segment of Zagros Fold-Thrust Belt in Kurdistan (Ibrahim, 2009; Burberry et al., 2010).

Aspect ratio and fold symmetry index for folds in this area are calculated from a fold map that is constructed from satellite images. The aspect ratio of folds varies from 6.1 to 13.7. The folds in the area are asymmetrical based on their symmetry index (Figure 5-11). In comparison with a study conducted by Burberry et al., (2010) on the Zagros

Simply Folded Belt in Iran, aspect ratio and fold symmetry index of these folds are located in a transition zone between fault-bend folds and fault-propagation folds. In addition, the presence of pure detachment folds is not expected based on their values of geomorphic indices (this study) and evidence from the field and restoration of cross-sections (Omar, 2005). Blanc et al. (2003) suggested the presence of both buckle folds and forced folds in the Iranian Zagros based on their aspect ratio. In this area, Safin and Peris Anticlines have the aspect ratios of 13.7 and 10.7 respectively. Safin and Peris Anticlines are good candidates for basement involvement and basement is known to be involved with the deformation in the Kurdistan Region through a number of reactivated transversal basement faults (Ameen, 1991 and 1992; Jassim and Goff, 2006). This may suggest the presence of a forcing member below these anticlines. Spatial distribution of folds in this segment of the fold belt is correlated with the spatial distribution of basement faults (Figure 5-10). However, as mentioned before, these folds may have been formed from lateral linkage of number of folds or segments. When folds link, their aspect ratio increases. In this situation, it is difficult to robustly differentiate between different types of folds from their geomorphic indices (Sattarzadeh et al., 2000; Burberry et al., 2010).

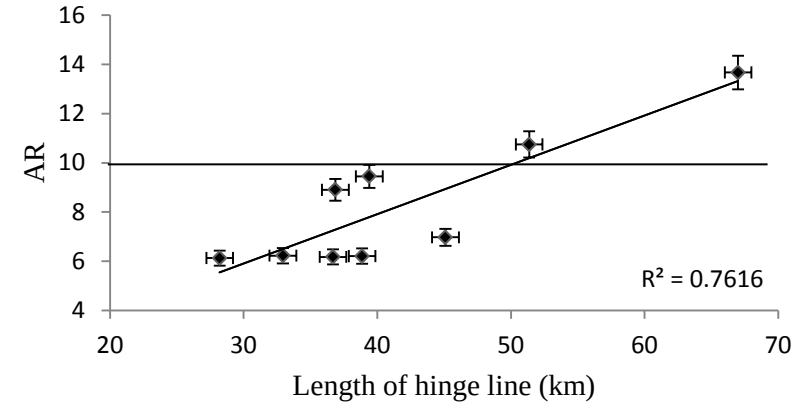

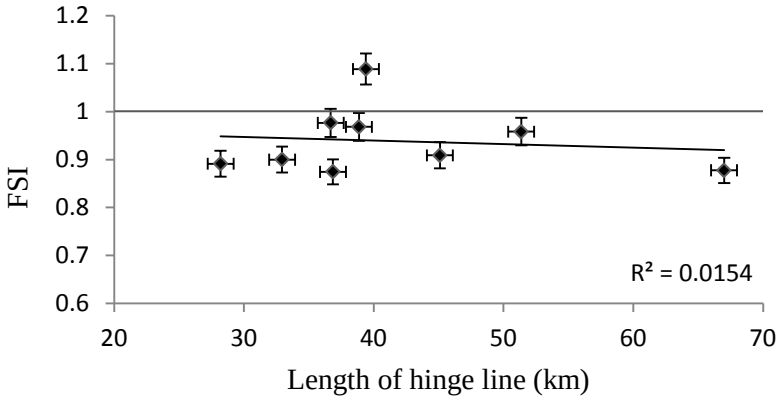

Figure 5-11: The relationship between length of hinge line with a) aspect ratio (AR) and b) fold symmetry index (FSI).

6-DISCUSSION

6.1 Geotectonic Setting

In this study, the geomorphic indices and geomorphic features of the folds in the study area suggest that these folds have been influenced by basement faults. The pre-Zagros structural elements have in the area include NW-SE trending Najd, NE-SW trending transversal and N-S trending Nabitah (less prominent in northern Iraq) Fault Systems (Ameen, 1992; Jassim and Goff, 2006; Aqrawi et al., 2010). The prominent right lateral transversal fault that runs along the Greater Zab River (Figures 2-3 and 5-10) separates the Mosul Block (to the west) from the Kirkuk Block (to the east). Due to a series of uplifts and erosional/non-depositional gaps during the Mesozoic in the Mosul Block, its sedimentary cover is thinner than the Kirkuk Block's sedimentary cover (Ameen, 1992). This difference in the thickness of the sedimentary cover between the two blocks may affect the geometry of the belt and deformations units e.g. fault dip, fault spacing and foreland-ward deformation propagation (Marshak and Wilkerson, 1992). Folds in the study area are parallel to NW-SE trending longitudinal basement faults. There are evidences of dip slip reverse movement on these faults at high angles (Ameen, 1991). These faults are thought to have been reactivated during the Zagros convergence (Jassim and Goff, 2006). Basement-rooted forced folds have a role in development of the folds in the Kirkuk Embayment (Ameen, 1991).

In this study, the calculated aspect ratio of some folds in the study area is more than 10 (Figure 5-11), and this may indicate presence of forcing member below these folds. This forcing member may be from a movement on the basement faults or a movement within the sedimentary cover (Cosgrove and Ameen, 2000). In this study,

Relatively low values of measured shortening across the folds in the constructed sections in this study, which are less than 30 % in most cases and consistent with those in a study by Omar (2005), indicates that the sedimentary cover is not totally decoupled from the Precambrian crystalline basement. The northwest extension of the Hormuz in the Kirkuk Embayment consists of clastic facies instead of salt (Kent, 2010; section 2.7.1), which is functioning as a basal detachment in the in the Iranian Zagros. This also supports the idea that the sedimentary cover is not able to be completely decoupled from the basement.

6.2 Detachment Levels

The sedimentary cover consists of c. 8 km thick rock units of rigid carbonate and clastic rocks interbedded with thin, weak units of shale and anhydrite (Figure 2-3). Based on the mechanical characteristics of sedimentary cover, mobile (incompetent) units, which may perform as detachments, are present in three levels: the Miocene Lower Fars Anhydrite, Triassic-Jurassic anhydrites and Ordovician-Silurian mudstones (De Vera et al. 2009; Aqrawi et al., 2010). The Lower Fars is an important detachment level in the Foothill Zone, but it has been eroded in the High Folded Zone, except in some areas within synclines. Thus, it does not influence the deformation style of the Cretaceous cored anticlines. In the synclines, the field data were collected within the Lower Fars and Upper Fars Formations and used to place pre-Lower Fars units at depth in the sections parallel to these domains. This may affect accuracy of the horizons drawn in synclines. The presence of thick mobile units such as shale or salt which may act as ideal detachment units has not been proven within the Mesozoic column. However, some units contain shale (Triassic Beduh and Baluti shales) and evaporites (Triassic Geli Khana and Kurra China) within their lithology. Also some units, which have evaporites and shales in

their lithology such as Adayah and Alan (Triassic) and Butmah (Jurassic), present in the Foothill Zone and absent in the Imbricated Zone (Jassim and Goff, 2006). These units may extend under parts of the High Folded Zone and act as possible detachments.

In this study, the calculated depth to detachment using area balancing method is within Triassic or older units. Presence of some errors is expected in this calculation because of complications introduced by related thrusts. In interpreted seismic lines in adjacent anticlines (e. g. Miran and Shaikhan Anticlines) with the High Folded Zone, detachment is located within the Triassic units (Heritage Oil Plc, 2010 and 2011; Gulf Keystone Petroleum LTD, 2013). The Triassic Kurra China Formation contains evaporites; the underlying Beduh Shale and overlying Baluti Shale are incompetent. Thus the detachment is placed within the Triassic units in this area. However, there is some thickening in the Jurassic units that contain anhydrites in core of anticlines (e.g. Perat Anticline; Figure 4-7). Thus, the cross-sections were constructed down to the Triassic. and the detachment within the Triassic units is emphasized.

The Infracambrian Hormuz Salt is not evidenced in the Kirkuk Embayment. The Ordovician-Silurian shales are proposed to be the lowest possible detachment level within the sedimentary cover (De Vera et al., 2009; Aqrawi et al., 2010). Consequently, deformation on multiple detachments has been proposed (De Vera et al. 2009; Aqrawi et al., 2010). However, precisely defining these levels of detachments requires further studies.

In seismic lines (Figures 4-7 and 4-8), the detachment is located within the Triassic or older units (~ 3 sec TWT). However, there is a thickening within the Jurassic units in the Perat Anticline in Bekhme (Figure 4-7). In the Miran (~45 km west of

Sulaimaniya) and Shaikhan (~50 km west of Akre) oil fields, which are located within the High Folded Zone, an interpreted seismic line shows that detachment is located within the Triassic or older units (Heritage Oil Plc, 2010 and 2011; Gulf Keystone Petroleum LTD, 2013; Appendix B). The Triassic Kurra China Formation contains evaporites in its lithology especially the upper part. In addition, other Triassic units such as the Baluti Shale which overlies the Kurra China and the Beduh Shale and Mirga Mir (limestone, shale, and evaporite) Formations which underlie the Kurra China Formation and Formation are incompetent (Jassim and Goff, 2006) and may act as detachment layers. The Kurra China Formation is equivalent to the Dashtak Formation in Iran (Sharland et al., 2001), which is considered as a possible detachment in the Dezful Embayment (Carruba et al., 2006; Fard et al., 2006).

6.3 Thick vs. Thin-Skinned Deformation

There are a number of ductile units within the sedimentary cover that have properties to work as a detachment for deformation of overlying units. The constructed structural cross-sections along the folds in the area (Figures 5-5 and 5-6) show deformation of the Tertiary, Cretaceous and Jurassic units above the Triassic units that are considered as a detachment. These may indicate the thin-skinned deformation in the area. However, the pre-Zagros structures (basement faults), which originated as normal faults and formed from extensional tectonic events, have divided northern Iraq to a number of blocks and sub-blocks and also affected the sedimentary basins via development of grabens and half grabens (Ameen, 1991 and 1992). Reactivation of the normal basement faults as reverse faults has been detected from geophysical evidence, field observation (Ameen, 1991) and geomorphology of folds (Ameen, 1991; this study).

Therefore, the combination of both thin-skinned and thick-skinned deformation is widely acceptable by many authors (Ameen, 1991; Ibrahim, 2009; De Vera et al., 2009) for this segment of the Zagros Fold-Thrust Belt.

6.4 Cross-Sections

The aspect ratio and fold symmetry index of these folds indicated that they are located in a transition zone between fault-bend fold and fault propagation folds. In addition, presence of pure detachment folds is not expected based on values of the aspect ratio and fold symmetry index (this study), evidence from the field and restoration of cross-sections (Omar, 2005). Thrusts were placed on the cross-sections, based on extrapolation from seismic lines and interpretation of the geomorphology and geometry of the associated folds and field observation. Thus, there is possibility of some imprecisions in the geometry and displacement along the thrusts. The rates of imprecisions can be reduced by further investigation on these folds using improved processing of seismic data. The displacement along blind thrusts decreases and dies upsection probably in soft layers due to simple shear within the layers or intersection of faults (e. g. intersection of faults in the Jurassic units in eastern side of the Perat Anticline; Figure 4-7). The Triassic-Jurassic units consist of carbonates in addition to layers of shale and evaporite. Therefore, variations in displacement along thrusts and in thicknesses in footwall and hanging wall are expected in incompetent shale and evaporite units. The same behaviors are expected in the Upper Cretaceous-Tertiary clastic rocks. Whereas, competent units such as the Cretaceous carbonates may act as ramp and thrusts break through them with minimum variations in displacement and change in thickness in the thrust walls.

In the crest of some anticlines, evidences of extension were found. These evidences include normal faults in crest of the Safin (field observation; Doski, 2002), Perat (field observation; Csontos, 2012) and Peris (field observation) Anticlines and crestal collapse in the Khatibian Anticline (field observation). These evidences support tangential longitudinal strain mechanisms of folding. Nevertheless, evidences of flexural folding such as layer parallel shear (Csontos, 2012) and interlayer slip (Reif et al., 2012) were found. Therefore, neither of these end-members folding mechanisms (tangential longitudinal strain or flexural folding) can be universally applied to the buckling of stratigraphic units in these folds, but contribution of both mechanisms is expected.

6.5 Lateral Growth of Folds and Along Strike Variations

The uplifting and folding in this segment of the Zagros Fold-Thrust Belt, which have started in the Early Miocene and propagated SW during the Pliocene (Csontos et al., 2012), led to erosion of about 2-3 km of the Cenozoic sediments, however, some the geomorphic evidence of fold growth have been preserved (Bretis et al., 2011; this study). In fold-thrust belts, there is a close connection between development of folds and associated blind thrusts (Keller et al., 1999). It is expected when the fault displacement increases, its lateral length increases at higher rates than the rate of displacement (Jackson et al., 1996; Keller et al., 1999; Ramsey et al., 2008). The geomorphic criteria used in this study (drainage network, water and wind gaps, long topographic profile of fold crest and fold front sinuosity) indicate northwest-ward propagation of the anticlines which are located in the eastern side of the area. In addition, the long topographic profile along a fold crest roughly reflects the amplitude along the fold and displacement rates along the associated thrust (Burbank and Anderson, 2012). Therefore, the long topographic profile

along fold crests in the study area (Figure 5-8) may reflect the displacement along the associated thrusts. In the Bani Bawi/Pirmam, Safin and Shakrok/Khatibian Anticlines, displacement rates along the thrusts in the southeastern and central segments that have higher long topographic profiles seem to be higher than the displacement rates in the northwestern segments that have lower long topographic profiles) of these anticlines where the Shaqlawa cross-section goes through (Figure 4-4).

Based on the geomorphology of the folds and direction of hinge lines, folds can be divided into a number of segments. These segments probably started as separate folds formed from separate thrusts. Then, they were propagated laterally with the evolution of deformation and linked to form one single linear fold or *en-echelon* folding style. Folds in the eastern side of the study area are located between two NE-SW trending transversal basement faults; one is right-lateral and runs along the Greater Zab River and the other is left-lateral runs along the Lesser Zab River to the SW (Figure 5-10). There is another right lateral fault between the two main faults, which separates the area into two sub-blocks (Omar, 2005). The segments of folds, which exhibit geomorphic evidence of lateral growth, are located within the western sub-block, despite the folds in the two sub-blocks are in the same distance to the backstop of the belt. Variations in the direction of hinge lines through the lateral growth of folds indicate changes in the stress direction with time. This is probably related to the rotation of the Arabian Plate (Omar, 2005). This means there is a close relation between lateral growth of folds and the basement faults.

6.6 Implications for Petroleum Systems

The Kurdistan Region, including the study area, is presently considered an important hydrocarbon province. The broad and box-shaped anticlines in the area are

indeed structures for accommodating hydrocarbons. The sealing capacity of associated thrusts must be considered carefully in these folds. Some associated faults in the adjacent anticlines to the study area (e. g. in Atrush Field; west to the Akre Anticline) exhibit trapping efficiency within the Jurassic and Triassic systems (Shamaran petroleum corp, 2012). Thus, the same efficiency is expected from most thrusts in the area. However, the lithology of the sedimentary units in both hanging wall and footwall has a role in the trapping efficiency of the thrusts. For instance, the Jurassic and Triassic units in the footwall block of the thrust in the southern limb of the Perat Anticline are facing the Triassic units (probably the Kurra China and Baluti Shale Formation) in the hanging wall (Figure 4-5). The anhydrite and shale in the Triassic units may seal the Triassic and Jurassic petroleum systems in the footwall. The younger Cretaceous system has been exposed to the surface due to uplift and erosion of Cenozoic units, which seal the Cretaceous system. This exposure led to seepage of the Cretaceous petroleum system through tertiary migration, as evidenced through bitumen seepage around these anticlines. Seepages are not detected along linear trends above thrusts or blind thrusts. This suggests that there is a chance of for these thrusts to seal hydrocarbons at deeper level in the sedimentary cover.

Folds in the area have grown laterally or they formed from linkage of separate segment. The fold growth and fold segments (i.e. location of linkage and lateral extension of fold segments) were affected by the distribution of the transversal basement faults in the area. Thus, traps within a single fold may be segmented via lateral growth of the fold and/ or influence of the basement faults.

7-CONCLUSIONS

The aims of this study were to address the geometry and formation mechanisms of a number of fault-related folds in the area, to identify possible detachment levels at depth, to estimate shortening across the folds in the area and to understand along strike variations in fold segments and their lateral growth. The first three aims of the study were met by constructing cross-sections that represent configuration model of deformation style of fold-related folds in the area via delineating the geometry of associated thrusts, identifying detachment levels, and estimating the shortening. In addition, the fourth aim was met by detecting lateral growth of a number of folds via geomorphic evidence.

This segment of the Zagros Fold-Thrust Belt is dominated by an *en-echelon* folding style. Folds are close to gentle, box-shaped with a broad to wide crest area. These folds are associated with thrusts in their forelimb and sometimes in their backlimb. Some thrusts are emergent while others remain as blind thrusts beneath the folds. The displacement along thrusts varies from tens of m up to more than 2500 m (e. g. thrust in southern limb of Akre and Perat Anticlines). Main associated thrusts are mostly dipping northeast-ward, which is consistent with the direction of deformation propagation (southwest-ward). However, sometimes the main thrusts are dipping southwest-ward, which is inconsistent with direction of deformation propagation. The dip of fold limbs often reflects the direction of main thrust. They are steeper in the limb that accommodates the thrust. Antithetic faults (or back thrusts) and synthetic faults occur in folds; normal faults also exist (e. g. northwestern limb of Shakrok Anticline). In addition, out-of-the syncline thrusts, which are considered fold-accommodation faults, are also detected in northern limb of Akre Anticline.

The structural style in the study area is interpreted to be from combination of both thin-skinned and thick-skinned deformation processes. Detachments occur at different levels within the sedimentary cover. The lowest detachment level is proposed to be within the Ordovician-Silurian shales. The dominant detachment level within the High Folded Zone is estimated to be within the Triassic units. However, some thickenings occur within the Jurassic units, which contain evaporite units. The aspect ratio of folds and fold symmetry index are 6:1-14:1 and 0.87-1.09 respectively, implying that folds are transitional between fault-bend folds and fault propagation folds. The aspect ratio of folds points toward presence of both buckle folds (AR<10) and forced folds (AR>10). The shortening along the constructed cross-sections is estimated at 12 % and 20-29 % in the Shaqlawa and Akre Sections respectively.

Variations in geometry of folds and associated faults occur along strike. In the Perat Anticline for instance, there is a change in the dip direction of the main thrust from SW in the eastern end to the N in the western end. This suggests that the anticline is located above the linkage of two faults. However, there is no obvious geomorphological indicator of linkage along it. Geomorphological criteria indicate variations along strike from detecting lateral propagation of folds. Most of these criteria indicate that the folds in eastern side of the area have been propagated west-ward. In the western side, there is no or little indicator of lateral growth only in parts close the fold tips. Based on geomorphology of the folds and direction of hinge lines, folds can be divided to number of segments. These segments probably started as separated folds from separated thrust. Then, they were propagated laterally with the evolution of deformation and linked to

form one single linear fold or *en-echelon* folding style. The lateral growth and spatial distribution of folds have a relation with the basement fault blocks.

Additional work, extending these methods to the wider Kurdistan Region, will further support conclusions reached in this study, detailed subsurface data should be included in any such studies.

References

Ahmadi, R., Ouali, J., Mercier, E., Mansy, J.-L., van-Vliet Lanoe, B., Launeau, P., Rhekhiss, F., and Rafini, S., 2006, The geomorphologic responses to hinge migration in the fault-related folds in the Southern Tunisian Atlas: Journal of Structural Geology, v. 28, p. 721-728.

Alavi, M., 2004, Regional stratigraphy of the Zagros Fold-Thrust Belt of Iran and its proforeland evolution: American Journal of Science, v. 304, p. 1-20.

Alavi, M., 2007, Structures of the Zagros fold-thrust belt in Iran: American Journal of Science, v., 307, p. 1064–1095.

Allen, M. B., Jackson, J., and Walker, R., 2004, Late Cenozoic reorganization of the Arabia-Eurasia collision and the comparison of the short term and long term deformation rates: Tectonics, 23, TC2008.

Al-Ameri, T. K., and Zumberge, J., 2012, Middle and Upper Jurassic hydrocarbon potential of the Zagros Fold Belt, North Iraq: Marine and Petroleum Geology, v. 36, p. 13-34.

Al-Juboury, A. I., and Al-Hadidy, A. H., 2009, Petrology and depositional evolution of the Paleozoic rocks of Iraq: Marine and Petroleum Geology, v. 26, p. 208–231.

Ameen, M. S., 1991, Possible forced folding in the Taurus-Zagros Belt of Northern Iraq. Geological Magazine, v. 128, p. 561-584.

Ameen, M. S., 1992, Effect of basement tectonics on hydrocarbon generation, migration and accumulation in northern Iraq: AAPG Bulletin, v. 76, p. 356-370.

Aqrawi, A. M., Goff, J. C., Horbury, A. D., and Sadooni, F. N., 2010, the Petroleum Geology of Iraq: Beaconsfield, UK, Scientific Press Ltd..

Azor, A., Keller, E. A., and Yeats, R. S., 2002, Geomorphic indicators of active fold growth: South Mountain–Oak Ridge anticline, Ventura basin, southern California: Geological Society of America Bulletin, v. 114, p. 745–753.

Bellen, R. C. Van, Dunington, H. V., Wetzel, R., and Morton D., M., 1959, Iraq.-Lexique Stratigraphique International, Paris, vol. III, Asie, Fascicule 10a.

Bahroudi, A., and Koyi, H. A., 2003, Effect of spatial distribution of Hormuz salt on deformation style in the Zagros fold and thrust belt: an analogue modelling approach: Journal of the Geological Society, London, v. 160, p. 719–733.

Berberian, M., 1995, Master ‘blind’ thrust faults hidden under the Zagros folds: active basement tectonics and surface morphotextonics: Tectonophysics, v. 241, p. 193-224.

Blanc, E. J. P., Allen, M. B., Inger, S., and Hassani, H., 2003, Structural styles in the Zagros Simple Folded Zone, Iran: Journal of the Geological Society, London, v. 160, p. 401–412.

Bretis, B., Bartl N., and Grasemann B., 2011, Lateral fold growth and linkage in the Zagros fold and thrust belt (Kurdistan, NE Iraq): Basin Research, v. 23, p. 615-630.

Buday, T., and Jassim, S. Z., 1987, The Regional geology of Iraq: tectonic, magmatism and metamorphism: Vol. 2, S.E.: Geol. Survey, Min. Invest., Baghdad, Iraq, p. 352.

Burbank, D. W., and Anderson, R. S., 2012, Tectonic Geomorphology: Wiley-Blackwell Science, Oxford.

Burbank, D. W., McLean, J. K., Bullen, M., Abdrakhmatov, K. Y., and Miller, M. M, 1999, Partitioning of intermontane basins by thrust-related folding, Tien Shan, Kyrgyzstan: Basin Research, v. 11, p. 75–92.

Burberry, C. M., Cosgrove, J. W., and Liu, J.-G., 2010, A study of fold characteristics and deformation style using the evolution of the land surface: Zagros Simply Folded Belt, Iran, in Leturmy, P., and Robin, C., Tectonic and Stratigraphic Evolution of Zagros and Makran during the Mesozoic–Cenozoic (eds): Geological Society of London, Special Publications no. 330, p. 139–154.

Carrruba, S., Perotti, C. R., Buonaguro, R., Calbro, R., Carpi, R. and Naini, M., 2006, Structural pattern of the Zagros fold-and-thrust belt in the Dezful Embayment (SW Iran): GSA. Special Publication, no. 414, p. 11-32.

Colman-Sadd, S. P., 1978, Fold development in Zagros simply folded belt, Southwest Iran:. AAPG Bulletin, v. 62, p. 984–1003.

Cooper, M., 2007, Structural style and hydrocarbon prospectivity in fold and thrust belts: a global review: Geological Society (London) Special Publication, no. 272, p. 447–472.

Cosgrove, J. W., and Ameen, M. S., 2000, A comparison of the geometry, spatial organization and fracture patterns associated with forced folds and buckle folds, In: Cosgrove, J. W. and Ameen, M. S. (eds) Forced Folds and Fractures: Geological Society, London, Special Publications, no. 169, p. 7–21.

Csontos, L., Sasvári, Á., Pocsai, T., Kósa, L., Salae A. T., and Ali, A., 2012, Structural evolution of the northwestern Zagros, Kurdistan Region, Iraq: Implications on oil migration: GeoArabia, v. 17, no. 2, p. 81-116.

Dahlstrom, C. D. A., 1969, Balanced cross sections: Canadian Journal of Earth Sciences, v. 6, p, 743-757.

Davis, G. H., Reynolds, S. J., and Kluth, C. F., 2011, Structural geology of rocks and regions, (3rd ed.): John Wiley and Sons, New Jersey.

De Vera, J., Gines, J., Oehlers, M., McClay, K., and Doski, J., 2009, Structure of the Zagros fold and thrust belt in the Kurdistan Region, northern Iraq: Trabajos de Geologia, Universidad de Oviedo, v, 29, p. 213-217.

Doski, J. A. H, 2002, Structural study along selected section across Safin Anticline (Kurdistan-Iraq): M. S. thesis, Salahaddin University, Erbil.

Fard, I. A., Braathen, A., Mokhtari, M., and Alavi, S. A. 2006, Interaction of the Zagros Fold–Thrust Belt and the Arabian-type, deep-seated folds in the Abadan Plain and the Dezful Embayment, SW Iran: Petroleum Geoscience, v. 12, p. 347–362.

Fleuty, M. J., 1964, The description of folds: Geological Association Proceeding, v. 75, p. 461-492.

Fogarasi, A., 2012, Operational update of our projects in Kurdistan Region of Iraq: MOL Group Investor Day, Budapest.

Fossen, H., 2010, Structural geology (2 ed.): Cambridge: Cambridge University Press.

Frehner, M., Reif, D., and Grasemann, B., 2012, Mechanical versus kinematical shortening reconstructions of the Zagros High Folded Zone (Kurdistan region of Iraq): Tectonics 31, TC3002.

Garland, C.R., Abalioglu, I. et al., 2010, Appraisal and development of the Taq Taq field, Kurdistan region, Iraq. In: Vining, B.A. & Pickering, S.C. (eds) Petroleum Geology: From Mature Basins to New Frontiers Proceedings of the 7th Petroleum Geology Conference:. Geological Society, London, v. 7, p. 801–810.

Ghasemi, A., and Talbot, C.J., 2005, A new tectonic scenario for the Sanandaj-Sirjan Zone (Iran): Journal of Asian Earth Sciences, xx, p. 1-11.

Gulf Keystone Petroleum LTD, 2013, Moving into development and production in the Kurdistan Region of Iraq: Natural Resource Forum.

Hessami, K., Koyi, H. A., Talbot, C. J., Tabasi, H., and Shabanian, E., 2001, Progressive unconformities within an evolving foreland fold-thrust belt, Zagros Mountains: Journal of the Geological Society of London, v. 158, p. 969-981.

Heritage Oil Plc, 2010, Kurdistan Technical Presentation.

Heritage Oil Plc, 2011, Kurdistan Technical Presentation.

Hossack, J. R., 1979, The use of balanced cross-section in the calculation of orogenic contraction, A review: Geological Society of London, v. 136, p.705-711.

Ibrahim, A. O., 2009, Tectonic Style and Evolution of the NW Segment of the Zagros Fold-Thrust Belt, Sulaimani Governorate, Kurdistan Region, NE Iraq: PhD thesis, University of Sulaimani, Sulaimani.

Jackson, J., Norris, R., and Youngson, J., 1996, The structural evolution of active fault and fold systems in central Otago, New Zealand: evidence revealed by drainage patterns: Journal of Structural Geology, v. 18, p. 217–234.

Jassim, S. Z., and Goff, J. C., 2006, Geology of Iraq: Dolin, Prague and Moravian Museum, Brno, Czech Republic.

Keller, E.A., Gurrola, L., and Tierney, T.E., 1999, Geomorphic criteria to determine direction of lateral propagation of reverse faulting and folding: Geology, v. 27, p. 515-518.

Kent, N., 2010, Structure of the Kirkuk Embayment, northern Iraq: Foreland structures or Zagros Fold Belt structures: GeoArabia, v. 15, no. 4, p. 147-188.

Marshak, S., and Wilkerson, M. S., 1992, Effects of overburden thickness on thrust belt geometry and development: Tectonics, v. 11, p. 560–566.

Marshak, S., and Wilkerson M. S. 2004, Fold-thrust belt-an essay, in: Ven Der Pluijm B. A., and Marshak S., (ed), Earth Structure, revised 2nd edition: Norton publishers, Ch. 18, p 444-474.

Marshak, S. and Woodward, N. B, 1988, Introduction to cross-section balancing, in Marshak, S., and Mitra, G., 1988, Basic methods of structural geology: Prentice Hall, New Jersey.

McQuarrie, N., 2004, Crustal scale geometry of the Zagros Fold-Thrust Belt, Iran: Journal of Structural Geology, v. 26, p. 519-535.

Mitra, S. 1990, Fault-propagation folds: geometry, kinematic evolution, and hydrocarbon traps: AAPG Bulletin, v. 74, p. 921–945.

Mitra, S., 2002, Fold-accommodation fault: AAPG Bulletin, v. 86, no. 4, p. 671-693.

Mitra, S., 2003, A unified kinematic model for the evolution of detachment folds: Journal of Structural Geology, v. 25, no. 10, p. 1659–1673.

Mitra, S., and Namson, J., 1989, Equal-area balancing: American Journal of Science, v. 289, no. 5, p.563-599.

Navabpour P., Angelier, J., and Barrier, E., 2008, Stress state reconstruction of oblique collision and evolution of deformation partitioning in W-Zagros (Iran, Kermanshah): Geophysical Journal International, v. 175, p. 755-782.

Numan, N. M. S., 1997, A plate tectonic scenario for the Phanerozoic succession in Iraq: Jour. Geol. Soc. of Iraq, v. 30 (2), p. 85-110.

Omar, A. A., 2005. An integrated structural and tectonic study of the Bina Bawi-Safin-Bradost Region: Ph.D. thesis, Salahaddin University, Erbil.

Petroceltic, 2013, A new MENA independent, January presentation.

Pitman, J. K., Steinshour, D., and Lewan, M. D., 2004, Petroleum generation and migration in the Mesopotamian basin and Zagros Fold Belt of Iraq, result from a basin modeling study: GeoArabia, v. 9, no. 4, p. 41-72.

Ramsey, J. G., 1967, Folding and fracturing of rocks: McGraw-Hill, New York.

Ramsey, L. A., Walker, R. T., and Jackson, J., 2008, Fold evolution and drainage development in the Zagros Mountains of Fars province, south-east Iran: Basin Research, v. 20, p. 23–48.

Reif, D., Decker, K., Grasemann, B., and Peresson, H., Fracture patterns in the Zagros fold-and-thrust belt, Kurdistan Region of Iraq: Tectonophysics, v. 576–577, p. 46–62.

Sattarzadeh, Y., Cosgrove, J., and Vita-Finzi, C., 2000, The Interplay of faulting and folding during the evolution of the Zagros deformation belt, In: Cosgrove, J. W. and Ameen, M. S. (eds) Forced Folds and Fractures: Geological Society, London, Special Publications, no. 169, p. 187–196.

Sella, G. F., Dixon, T. H., and Mao, A. 2002, REVEL: A model for Recent plate velocities from space geodesy: Journal of Geophysical Research, v. 107, No. B4, 2081, p. 30.

Sissakian, V. K., 1997, Geological map of Arbeel and Mahabad Quadrangles, 1: 250.000: State Establishment of Geological Survey and Mining, Iraq. Baghdad.

Sissakian, V. K., 2013, Geological evolution of the Iraqi Mesopotamia Foredeep, inner platform and near surroundings of the Arabian Plate: Journal of Asian Earth Sciences, v. 72, p. 152–163.

Shamaran Petroleum corp, Appraisal and development in Kurdistan: Corporate Presentation.

Sharland, P. R., Archer, R., Casey, D. M., Davies, R. B., Hall, S. H., Heward, A.P., Horbury, A. D., and Simmons, M. D., 2001, Arabian Plate sequence stratigraphy: GeoArabia Special Publication 2, Gulf PetroLink, Bahrain.

Sherkati, S., Molinaro, M., de Lamotte, D. F., and Letouzey, J., 2005, Detachment folding in the central and eastern Zagros folded-belt (Iran): salt mobility, multiple detachments and late basement control: Journal of Structural Geology, v. 27, p. 1680–1696.

Stern, R. J., and Johnson P., 2010, Continental lithosphere of the Arabian Plate: A geologic, petrologic, and geophysical synthesis: Earth-Science Reviews, v. 101, p. 29–67.

Suppe, J., 1983, Geometry and kinematics of fault-bend folding: American Journal of Science, v. 283, no. 7, p. 684–721.

Talebian, M., and Jackson, J., 2002, Offset on the main recent fault of NW Iran and implications for the late Cenozoic tectonics of the Arabia-Eurasia collision zone: Geophys. J. Int., v. 150, p. 422-439.

Tucker, C. j., Grant, D. M., and Dykstra, J. D., 2004, NASA's global 0rthorectified Landsat data set: Photogrammetric Engineering & Remote Sensing, V. 70, no. 3, p. 313–322.

Twiss, R. J., and Moores, E. M., 2007, Structural geology, 2nd ed.: New York: W. H. freeman and company.

Woodward, N. B., Boyer, S. E., and Suppe, J., 1989, Balanced geological cross-sections: an essential technique in geological research and exploration: Short Course Geol. Ser., AGU, Washington, D. C., v. 6, p. 132.

Yilmaz, Y. 1993, New evidence and model on the evolution of the southeast Anatolian Orogen: Geological Society of America Bulletin, v. 105, p. 251–271.

APPENDIX

Appendix A: Field Data

A.1: Field data along the Shaqlawa Section.

X (UTM)	Y (UTM)	Z (m)	Dip	Dip Dir.	Geo. Unit	Note
441248.3	4051906	822	15	19	Shiranish	
441203.1	4051842	830	11	30	Shiranish	
441150.7	4051808	842	15	17	Shiranish	
441162.7	4051744	859	10	46	Shiranish	
441085.2	4051667	882	10	30	Bekhme	
440988	4051631	891	18	40	Bekhme	
440933	4051576	901	2	50	Bekhme	
440772.9	4051420	931	9	36	Bekhme	
440678.1	4051359	946	6	49	Bekhme	
440605.5	4051285	956	9	43	Bekhme	
440510.5	4051193	974	9	39	Bekhme	
440435.6	4051135	989	11	37	Bekhme	
440382.9	4051065	996	8	35	Bekhme	
440320.3	4050998	988	4	235	Bekhme	
440235.6	4050961	988	6	242	Bekhme	
440153.4	4050928	981	4	328	Bekhme	
440076.1	4050888	983	6	307	Bekhme	
440026.1	4050852	980	5	270	Bekhme	
439946.4	4050828	975	4	52	Bekhme	
439891.6	4050794	986	10	290	Bekhme	
439839	4050742	974	12	280	Bekhme	
439801.6	4050721	934	12	240	Bekhme	
439741.7	4050684	913	11	245	Bekhme	
439689.4	4050666	882	16	225	Bekhme	
439652	4050654	881	21	226	Bekhme	
439602.1	4050624	846	23	234	Bekhme	
439539.8	4050596	812	25	260	Bekhme	

439477.5	4050569	788	27	264	Bekhme	
439412.7	4050539	755	26	252	Bekhme	
439360.3	4050502	730	24	260	Bekhme	
439290.6	4050484	706	17	252	Bekhme	
439552.3	4049191	722	20	240	Bekhme	
439462.5	4049139	688	29	253	Bekhme	
439305.7	4049113	671	64	56	Shiranish	Overturned
439089	4049040	645	73	234	Kolosh	
438914.1	4048909	701	50	233	Pila Spi	
438839.3	4048863	669	51	233	Pila Spi	
438579	4048616	628	28	221	Lower Fars	
438464.1	4048524	636	29	233	Lower Fars	
436715.1	4046922	568	25	246	Upper Fars	
435971.3	4046179	538	19	240	Upper Fars	
435903.6	4046108	542	15	233	Upper Fars	
435840.8	4046022	531	17	239	Upper Fars	
435894.7	4045908	525	15	237	Upper Fars	
435799.7	4045835	532	13	233	Upper Fars	
435722.4	4045808	537	15	224	Upper Fars	
435664.8	4045756	530	13	235	Upper Fars	
435581.9	4045633	499	11	217	Upper Fars	
435514.1	4045541	490	11	238	Upper Fars	
436195	4044168	521	9	255	Upper Fars	
435962.6	4044003	540	5	277	Upper Fars	
435728.8	4043672	558	35	38	Upper Fars	
435666	4043589	572	16	30	Upper Fars	
435620.8	4043528	580	41	25	Upper Fars	
435574.8	4043359	591	46	24	Upper Fars	
435529.3	4043264	617	45	24	Upper Fars	
435491	4043132	611	47	30	Upper Fars	
435457.8	4043012	606	47	28	Upper Fars	
435432.3	4042922	602	44	30	Upper Fars	
435406.4	4042784	614	51	24	Upper Fars	

435315.5	4042609	627	45	22	Upper Fars	
435287.4	4042501	650	38	11	Upper Fars	
435254.2	4042385	678	35	31	Lower Fars	
435185.3	4042157	713	39	22	Lower Fars	
435172.3	4042077	719	38	13	Lower Fars	
435096.5	4041920	700	48	24	Lower Fars	
435068.5	4041837	709	29	17	Lower Fars	
435044.7	4041647	742	33	22	Pila Spi	
434993.8	4041502	796	34	13	Pila Spi	
434649.5	4041690	811	55	8	Pila Spi	
434640.2	4041449	878	38	355	Pila Spi	
434457.8	4041334	888	22	8	Pila Spi	
434583.5	4041191	927	24	6	Pila Spi	
434502.4	4040991	962	18	0	Pila Spi	
434489.5	4040924	974	15	9	Pila Spi	
434448.6	4040782	982	14	13	Pila Spi	
434398.1	4040690	989	13	310	Pila Spi	
434370.4	4040641	991	5	326	Pila Spi	
434239.7	4040457	1034	11	323	Pila Spi	
434184.2	4040359	1036	7	310	Pila Spi	
434158.5	4040254	1040	9	292	Pila Spi	
434142.8	4040159	1047	9	276	Pila Spi	
434189.4	4040060	1055	3	283	Pila Spi	
434218.5	4039970	1064	6	338	Pila Spi	
434252.5	4039862	1078	8	302	Pila Spi	
434301.5	4039754	1084	6	258	Pila Spi	
434298.2	4039658	1078	7	236	Pila Spi	
434259.8	4039511	1072	9	331	Pila Spi	
434209	4039373	1069	13	257	Pila Spi	
434200.9	4039296	1071	20	313	Pila Spi	
434150.3	4039185	1066	12	294	Pila Spi	
434115	4039121	1077	11	283	Pila Spi	
434094.7	4039068	1066	8	235	Pila Spi	

434074.2	4038985	1066	5	234	Pila Spi	
434046.2	4038909	1060	7	246	Pila Spi	
433990.8	4038813	1045	10	233	Pila Spi	
433947.7	4038712	1043	6	237	Pila Spi	
433919.9	4038654	1013	12	233	Pila Spi	
433871.5	4038519	999	12	248	Pila Spi	
433816.4	4038467	980	12	244	Pila Spi	
433700.8	4038323	1009	17	215	Pila Spi	
433545.9	4038231	956	20	225	Pila Spi	
436458.2	4035667	1010	27	216	Pila Spi	
436415	4035550	968	27	213	Pila Spi	
436382.2	4035492	923	33	203	Pila Spi	
436351.9	4035434	902	32	211	Pila Spi	
436286.7	4035373	888	43	208	Pila Spi	
436219.2	4035321	834	31	207	Pila Spi	
436138.2	4035140	858	35	213	Lower Fars	
435992.6	4034977	833	33	203	Lower Fars	
435941.8	4034842	779	36	209	Lower Fars	
435921.2	4034753	765	47	214	Upper Fars	
435863.3	4034661	729	32	208	Upper Fars	
436155.1	4034400	739	34	210	Upper Fars	
435994.4	4034219	732	28	207	Upper Fars	
435843.7	4034032	707	17	200	Upper Fars	
435773.1	4033913	718	54	47	Upper Fars	
435597.5	4033738	790	54	30	Lower Fars	
435557.1	4033662	833	53	47	Lower Fars	
435534.4	4033622	846	63	40	Lower Fars	
435516.6	4033566	883	65	41	Lower Fars	
435438.8	4033490	917	76	46	Lower Fars	
435355.8	4033370	937	41	35	Lower Fars	
435305.6	4033315	959	28	48	Lower Fars	
435218.1	4033264	977	54	48	Pila Spi	
435160	4033156	1015	42	52	Pila Spi	

434995.7	4033164	1052	53	36	Pila Spi	
434927.9	4033078	1045	30	30	Gercus	
434905	4033016	1016	44	45	Gercus	
434749.3	4032839	997	50	50	Kolosh	
434646.6	4031108	893	3	23	Shiranish	
434556.2	4031010	900	4	350	Shiranish	
434365.5	4030830	905	6	12	Bekhme	
434327.5	4030737	903	13	215	Shiranish	
434109.3	4030533	878	19	236	Shiranish	
434017.6	4030275	855	17	203	Shiranish	
433963.8	4030068	846	32	230	Shiranish	
433534.6	4029317	846	51	236	Kolosh	
433141.5	4029052	861	48	234	Pila Spi	
433016.8	4029037	863	44	229	Pila Spi	
432896.7	4028967	853	33	228	Lower Fars	
432671.7	4028867	845	17	235	Lower Fars	
432306.9	4029354	871	33	225	Lower Fars	
432196.9	4029306	852	19	222	Lower Fars	
432066.8	4029230	905	27	250	Upper Fars	
431828.7	4029047	841	7	228	Lower Fars	
431658.5	4028940	811	0	223	Lower Fars	
431510.9	4028858	803	6	38	Lower Fars	
431397.9	4028745	808	11	27	Lower Fars	
431322.7	4028687	802	11	60	Lower Fars	
430454.7	4027927	789	17	43	Lower Fars	
429747.7	4028299	836	11	67	Pila Spi	
429584.9	4028186	861	11	12	Pila Spi	
429722.1	4027902	879	9	50	Pila Spi	
429807.8	4027719	895	8	43	Pila Spi	
429869.9	4027398	910	8	72	Pila Spi	
429547	4027509	929	12	51	Pila Spi	
429222.1	4027690	993	7	31	Pila Spi	
429107.8	4027432	992	10	53	Pila Spi	

429101.3	4027244	1009	10	42	Pila Spi	
429039.4	4026980	1026	12	46	Pila Spi	
428108	4025539	1033	6	239	Pila Spi	
427826.2	4025215	1004	7	234	Pila Spi	
427575.8	4025069	989	11	250	Pila Spi	
427350.6	4024963	961	7	210	Pila Spi	
427388.4	4024716	928	9	252	Pila Spi	
427343	4024643	920	9	232	Pila Spi	
427117.9	4024552	867	12	242	Pila Spi	
427123.7	4024352	855	19	235	Pila Spi	
427075.7	4024281	828	17	222	Pila Spi	
427099.5	4024146	815	13	232	Pila Spi	
426719.8	4023742	760	19	234	Lower Fars	

A.2: Field data along the Akre Section.

X (UTM)	**Y (UTM)**	**Z (M)**	**Dip**	**Dip Dir.**	**Geo. Unit**	**Note**
412879.16	4064859.6	645	56	350	Upper Fars	Overturned
412880.04	4064945.8	646	56	3	Upper Fars	Overturned
412911.06	4065068.8	646	65	0	Lower Fars	Overturned
412941.58	4065142.5	659	59	345	Lower Fars	Overturned
412949.8	4065219.4	677	42	340	Lower Fars	Overturned
412913.94	4065352.3	702	50	10	Lower Fars	Overturned
412894.63	4065404.9	723	56	0	Lower Fars	Overturned
412910.99	4065549.6	763	58	173	Pila Spi	
413182.13	4065623.9	788	59	176	Pila Spi	
413284.53	4065937.2	853	35	169	Khurmala/Kolosh	
413285.78	4066060.4	891	33	178	Khurmala/Kolosh	
413286.4	4066122	905	31	170	Khurmala/Kolosh	
413291.99	4066183.6	918	20	195	Khurmala/Kolosh	
413340.26	4066297.2	960	23	198	Khurmala/Kolosh	
413353.32	4066361.7	969	26	172	Khurmala/Kolosh	
413353.79	4066408	990	24	178	Khurmala/Kolosh	

413326.82	4066439.1	995	14	205	Khurmala/Kolosh	
413317.15	4066463.8	1007	15	198	Khurmala/Kolosh	
413081.95	4066506.3	1027	20	142	Khurmala/Kolosh	
413065.16	4066561.9	1043	16	145	Khurmala/Kolosh	
413015.21	4066772	1055	2	200	Khurmala/Kolosh	
413018.16	4067061.6	1081	5	198	Khurmala/Kolosh	
412967.24	4067176.2	1099	1	180	Khurmala/Kolosh	
413000.86	4067311.4	1118	5	28	Khurmala/Kolosh	
413008.04	4067530.2	1105	15	210	Khurmala/Kolosh	
413026.56	4067644	1107	9	167	Khurmala/Kolosh	
412995.67	4067776.8	1137	5	195	Khurmala/Kolosh	
412965.85	4068014.4	1160	10	173	Khurmala/Kolosh	
412961.55	4068079.2	1162	12	160	Khurmala/Kolosh	
412937.98	4068199.6	1138	4	218	Khurmala/Kolosh	
413317.73	4068232.8	1183	0	360	Khurmala/Kolosh	
413290.88	4068519.6	1161	11	305	Khurmala/Kolosh	
413140.76	4068632.1	1152	14	301	Khurmala/Kolosh	
413041.02	4068821.1	1120	47	160	Khurmala/Kolosh	
412985.78	4068997.3	1088	12	252	Aqra	
412864.8	4069047.9	1057	8	255	Aqra	
412800.9	4069104	1033	26	290	Aqra	
412717.14	4069157.2	994	17	315	Aqra	
412623.66	4069229.1	968	13	346	Aqra	
412575.21	4069340.5	941	17	358	Aqra	
412608.92	4069485	931	64	338	Aqra	
412629.79	4069586.5	910	60	351	Khurmala/Kolosh	
412657.79	4069657.1	887	45	358	Khurmala/Kolosh	
412671.03	4069740.2	855	39	2	Khurmala/Kolosh	
412679.13	4069804.8	834	41	18	Khurmala/Kolosh	
412722.06	4069881.4	785	43	7	Khurmala/Kolosh	
412715.79	4069995.5	806	51	5	Pila Spi	
412746.33	4070072.2	785	62	7	Lower Fars	
412760.11	4070207.7	762	54	1	Lower Fars	

412756.09	4070300.2	755	52	6	Lower Fars	
412766.51	4070349.4	759	71	7	Lower Fars	
412789.74	4070438.5	741	59	17	Lower Fars	
412807.69	4070496.9	725	67	2	Upper Fars	
412806.37	4070610.9	724	52	7	Upper Fars	
412819.49	4070681.7	721	57	13	Upper Fars	
412835.31	4070774	700	52	8	Upper Fars	
412841.49	4070894.1	710	55	9	Upper Fars	
412877.1	4070983.1	710	64	10	Upper Fars	
412942.4	4071065.7	715	55	15	Upper Fars	
412970.23	4071120.9	726	57	13	Upper Fars	
412983.35	4071191.6	741	61	14	Upper Fars	
412993.22	4071333.1	718	64	7	Upper Fars	
413022.69	4071403.8	740	73	18	Upper Fars	
413053.06	4071465.2	759	83	183	Upper Fars	
413068.72	4071542.1	768	79	209	Upper Fars	
413126.89	4071655.5	750	87	25	Upper Fars	Overturned
413179.97	4071756.7	790	78	16	Upper Fars	Overturned
413185.49	4071812.1	792	88	199	Upper Fars	
413204.38	4071962.9	799	80	212	Upper Fars	
413229.82	4072027.3	805	77	204	Upper Fars	
413250.34	4072094.9	824	54	205	Upper Fars	
413272.89	4072119.4	840	83	202	Lower Fars	
413298.15	4072165.3	840	75	201	Lower Fars	
413323.68	4072239	841	87	206	Lower Fars	
413369.58	4072364.9	870	78	200	Lower Fars	
413425.38	4072490.7	905	86	201	Lower Fars	
413453.45	4072570.6	955	63	200	Pila Spi	
414080.61	4072333.1	936	57	196	Pila Spi	
414114.16	4072465.3	913	69	203	Khurmala/Kolosh	
414199.51	4072572.3	962	66	215	Aqra	
414264.59	4072636.3	1009	63	198	Aqra	
414319.92	4072715.9	1049	61	195	Aqra	

414323.08	4072783.7	1026	67	206	Aqra	
414343.86	4072879	1002	64	204	Aqra	
414408.43	4072644.1	1042	65	199	Aqra	
414456.71	4073010.4	1040	67	203	Aqra	
414457.27	4073065.8	1030	59	211	Aqra	
414480.28	4073136.5	1035	65	203	Aqra	
414555.55	4073228.2	1082	82	202	Qamchuqa	
414598.05	4073264.8	1121	85	205	Qamchuqa	
414665.82	4073350.4	1154	28	198	Qamchuqa	
414714.29	4073488.6	1153	40	205	Qamchuqa	
414754.92	4073586.8	1192	46	202	Qamchuqa	
414780.07	4073623.5	1145	45	199	Sarmord/Garagu	
414842.85	4073706.1	1083	45	196	Sarmord/Garagu	
414853.75	4073804.6	1059	35	206	Sarmord/Garagu	
414958.44	4074114.8	908	70	350	Sargelu//Naokelekan/ Barsarin/Chia Gara	
414981.57	4074197.8	851	39	212	Sargelu//Naokelekan/ Barsarin/Chia Gara	
415089.5	4074335.4	835	35	197	Sarki/Sehkaniyan	
415125.26	4074442.9	826	22	209	Sarki/Sehkaniyan	
415178.49	4074562.6	806	12	197	Sarki/Sehkaniyan	
415261.14	4074651.1	772	16	200	Sarki/Sehkaniyan	
415328.98	4074746	778	10	202	Sarki/Sehkaniyan	
415391.81	4074834.7	781	0	202	Sarki/Sehkaniyan	
415462.13	4074929.6	760	0	23	Sarki/Sehkaniyan	
415536	4075132.2	726	10	23	Sarki/Sehkaniyan	
415643.48	4075226.7	764	10	1	Sarki/Sehkaniyan	
415659.32	4075325.2	746	88	19	Sarki/Sehkaniyan	
416300.44	4075263.4	702	85	17	Sargelu//Naokelekan/ Barsarin/Chia Gara	
416331.34	4075383.3	676	86	23	Sargelu//Naokelekan/ Barsarin/Chia Gara	
416344.91	4075503.3	685	87	28	Sarmord/Garagu	

416400.77	4075641.4	663	67	215	Sarmord/Garagu	Overturned
416496.09	4075760.7	652	84	192	Sarmord/Garagu	Overturned
416552.49	4075954.3	633	73	208	Qamchuqa	Overturned
416635.06	4076036.7	668	86	22	Qamchuqa	
416695.66	4076153.2	684	75	10	Aqra	
416736.07	4076233	688	83	21	Aqra	
416766.58	4076312.8	699	86	21	Aqra	
416782.77	4076448.2	657	83	24	Aqra	
416798.44	4076531.3	637	83	25	Aqra	
416187.3	4076860.9	709	88	22	Aqra	
416236	4077026.8	673	70	25	Aqra	
416348.32	4077364.7	678	52	23	Aqra	
416386.56	4077475.3	712	17	50	Aqra	
416413.11	4077656.8	717	10	87	Aqra	
416462.53	4077896.7	696	10	345	Aqra	
416469.32	4078084.6	654	15	355	Aqra	
416376.75	4078242.7	585	12	174	Aqra	
416414.51	4078304	598	11	171	Aqra	
416462.5	4078399.1	604	10	355	Aqra	
416451.78	4078568.7	592	5	166	Aqra	
416539.27	4078903.7	519	9	11	Shiranish	

Appendix B: Used Seismic Lines

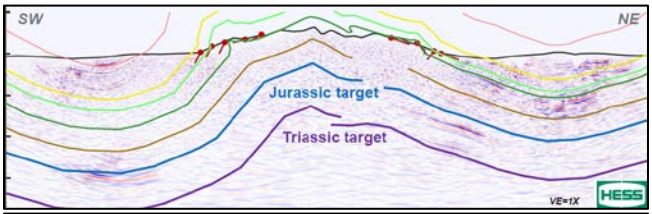

B 1: seismic line across the western side of the Shakrok Anticline. (Petroceltic, 2013).

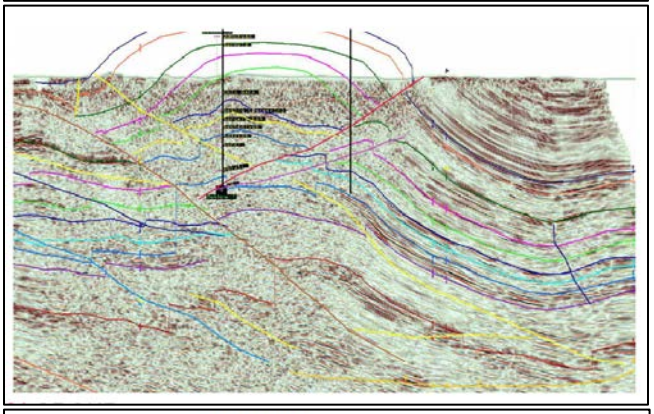

B 2: Seismic line across the eastern side of the Perat Anticline in Bekhme. (Fogarasi, 2012).

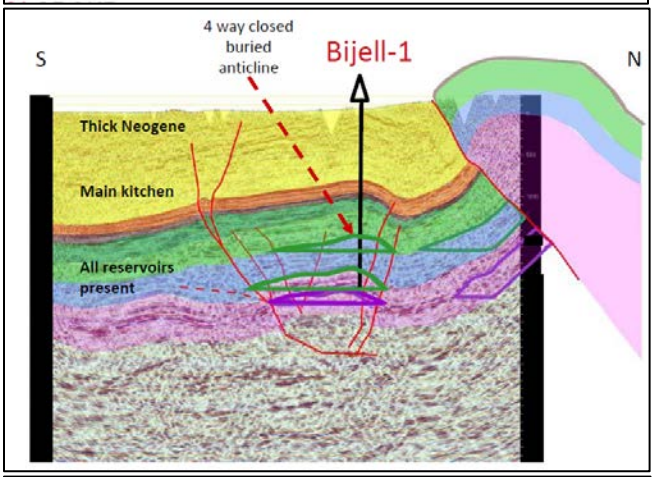

B 3: Seismic line across the western side of the Perat Anticline in Bekhme. (Fogarasi, 2012).

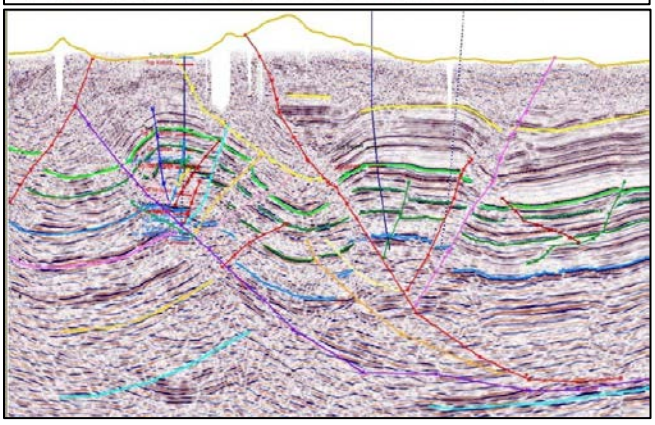

B 4: Seismic line across Miran structure (~45 km west of Sulaimaniya; Heritage Oil Plc, 2010)